Chapter 6

Potential geodetic signals from other sources

Understanding the various processes that contribute to local and global sea-level changes is a fundamental part of the climate change debate. But variations in observed sea level and the deformation of the Earth surface are caused by many factors and the challenge is to separate the various contributions. Geodetic signals of the response to recent mountain deglaciation are the main focus of this thesis and were discussed in the previous chapters. However, in order to fully understand the geodetic observations and successfully model them, all other contributing factors of the variations must be accounted for. The Earth's response and sea-level change to many of these processes are of a similar nature as the problem addressed previously of recent mountain deglaciation, i.e. resulting from redistribution of mass on the Earth's surface, such as sediment or volcanic loading or groundwater and surface water redistribution. This chapter will address some of these factors.

Large parts of the Earth's crust are subject to active tectonics. The degree to which these tectonic processes affect the geodetic signals vary greatly from location to location. Section 6.1 focuses on the impact that tectonic activity has on geodetic signals in Alaska where deglaciation signals area also important. Section 6.2 discusses the contribution to recent and present sea-level rise due to volume changes in the Antarctic and Greenland ice sheets. The deglaciation following the Last Glacial Maximum and the Little Ice Age may have ongoing effects on geodetic signals to a significant level and are discussed in Section 6.3. Changes in terrestrial water storage and their impact on geodetic signals are discussed in Section 6.4. Thermal expansion, believed to be the biggest factor in terms of contribution

to present-day global sea-level rise, is addressed in Section 6.5. The first order contribution of this effect may be easily estimated but second order effects due to the redistribution of water masses caused by non-uniform thermal expansion of the oceans may be significant at the level of current measurements and are discussed in the same section. Section 6.6 summarizes the significance of the various processes which contribute to present-day variations of geodetic observations.

6.1 Tectonics

Plate tectonics can result in considerable surface movements, as observed in active mountain chains, and consequently will have a large effect on local sea level in such regions. A detailed study of the impact that plate tectonics has on the geodetic signals is beyond the scope of this thesis. Hence, only one example of tectonic movements, in Alaska where various studies have been undertaken, is presented below. This region has been chosen because of the major deglaciation taking place at nearby mountain ranges. Hence, it becomes interesting whether it is possible to separate the two signals in the observations.

The coastal area in south Alaska is particularly susceptible to plate tectonic processes as it lies on the boundary between the Pacific and North-American plates where plate movements of various kind are taking place (Figure 6.1). Strike-slip motion[1] occurs along the Fairweather-Queen Charlotte fault (FW-QC), while the Pacific plate is subducted beneath North America along the Aleutian Megathrust (AMT). A micro-plate (the Yakutat Block) is actively colliding with North America at the transition from strike-slip to subduction. The western portion of the Yakutat Block is partially being subducted in the Kayak Island and Pamplona Zones (KI-PZ), while crustal shortening accommodates relative plate motion at the eastern corner in the St. Elias Mountains. The Yakutat Block is bounded to the south by the Transition Zone (TZ). Minor strike-slip motion occurs along the Denali fault (DF) within the North-American plate.

In regards to the effects caused by mountain deglaciation, vertical movements are of greatest interest and hence, from the tectonic setting of Figure 6.1, it can be inferred that the area where the Pacific Plate is subducting under the North-American plate potentially has the largest vertical displacements. There is no subduction to the east because the relative plate movements are predominately

[1]The fault surface of a strike-slip fault is usually near vertical and the footwall moves horizontally with very little vertical motion.

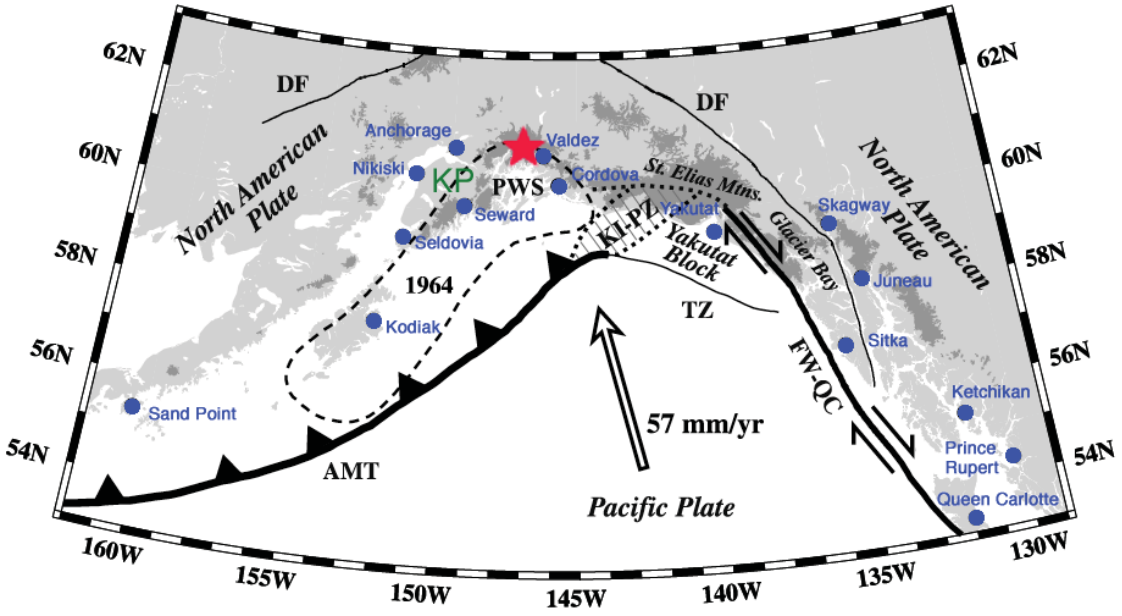

Figure 6.1: Tectonic setting in Alaska (Larsen et al., 2003). The open arrow indicates the velocity of the Pacific Plate relative to North-American Plate. Dark grey areas represent the locations of glaciers.

strike-slip (i.e. horizontal) and therefore there is no major driving mechanism for vertical crustal displacements.

The *Great Alaskan Earthquake* of 1964 (Eckel, 1970) was the largest earthquake in North America and the second largest ever recorded (largest occurred in Chile in 1960). The epicenter (red star in Figure 6.1) was in the Northern Prince William Sound (61.1°N / 147.7°W) about 120 km east of Anchorage. The reported Richter magnitudes for this earthquake range from 8.4 to 8.6. The moment magnitude[2] is reported as 9.2 (Kanimori, 1977). The depth where the rupture began was approximately 23 km within the Earth's crust. Ground deformations were extensive with some areas east of Kodiak being raised by 9 meters and areas around Portage (70 km south-east of Anchorage) being dropped by almost 2.5 meters (Plafker, 1969)[3]. The rupture area of the 1964 earthquake inferred from aftershocks, is enclosed by the dashed line in Figure 6.1. It represents the plate interface where the North-American and Pacific plates interact.

Freymueller et al. (2000) studied the spatial variation of present-day deformation at the Kenai Peninsula (indicated as KP in Figure 6.1) in Alaska. GPS measurements taken over four years show that the eastern Kenai Peninsula is migrating in a NNW direction, whereas the western Kenai Peninsula is moving in a SE direction.

[2]moment magnitude provides a better measure of energy release for larger earthquakes
[3]and http://wcatwc.arh.noaa.gov/64quake.htm

Velocities on the eastern side range from ∼55 mm year^{-1} in southern Prince William Sound to ∼30 mm year^{-1} at Seward and ∼5 mm year^{-1} near Anchorage. The velocities at the western Kenai Peninsula are of the order of 20 mm year^{-1}. These observations support the model in Freymueller et al. (2000) that assumes a sharp contrast in the coupling between the upper and lower plates in the eastern and western Kenai profiles (i.e. the plate interface beneath the eastern Kenai is completely or almost completely locked, whereas beneath the western Kenai, the plate interface appears to be slipping freely). The study by Freymueller et al. (2000) also indicated significant post-seismic uplift over most of the regions which subsided during the earthquake. Uplift rates determined from GPS measurements over the period 1993-1997 are up to 30 mm year^{-1} over the Kenai Peninsula (Figure 6.2).

Cohen and Freymueller (2001) examined tide gauge measurements to determine the history of crustal movements subsequent to the 1964 earthquake. Observed sea-level rates are corrected for local oceanographic and atmospheric effects (after the procedure outlined in Savage and Plafker, 1991) as well as for post-glacial rebound (by applying ±1 mm year^{-1} along the south coast of Alaska, as derived by Peltier and Tushingham, 1989), and eustatic sea-level change (by adding the somewhat arbitrary amount of 2 mm year^{-1}). Uplift rates of 10 mm year^{-1} or more occur at tide gauge sites at the western side of the Kenai Peninsula. As these uplift rates have persisted for at least 35 years, Cohen and Freymueller (2001) concluded that these movements are due to long-lived post-seismic activity. At the eastern side of the Kenai Peninsula, slow uplift rates of only a few millimetres per year occur (Cohen and Freymueller, 2001).

Larsen et al. (2003) studied sea-level records from 15 tide gauge stations along the northern North American - Pacific plate boundary to measure rates of uplift. On the eastern side where strike-slip motion dominates, rates of uplift are small, whereas areas with major glacial unloading have experienced extremely rapid uplift. At the station Yakutat, located in the transition zone between strike-slip and subduction, the record shows a high uplift rate of non-linear character due to tectonic influences. On the western side, in the subduction zone, vertical crustal motions are predominantly non-linear. Records exhibit significant shifts superimposed on the records at the times of major earthquakes and several phases of postseismic deformation (Larsen et al., 2003).

The above studies illustrate that plate tectonic processes can have significant effects on geodetic signals and that these variations in horizontal and vertical movements are strongly dependent on the location. The case study of Alaska show that tectonic

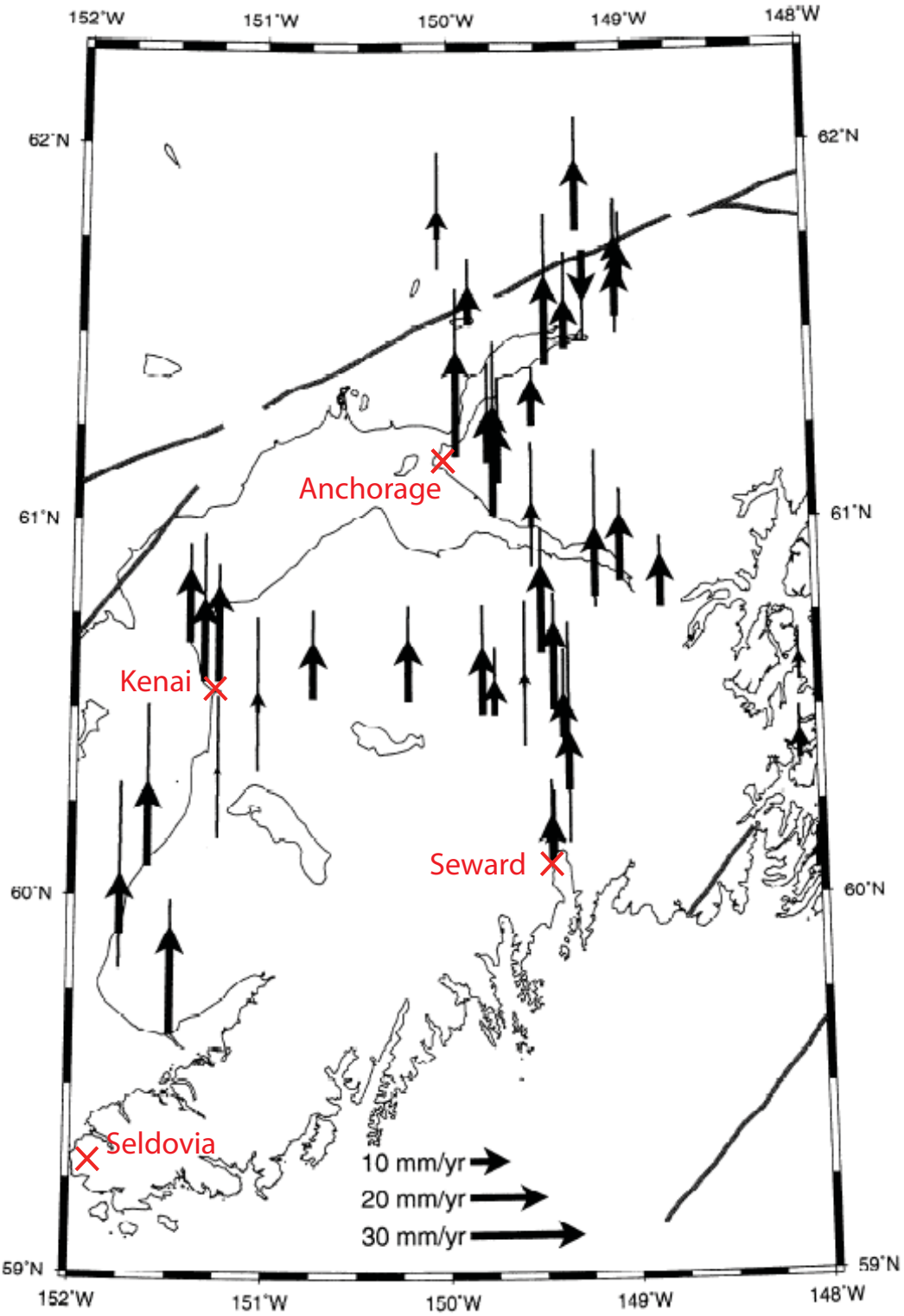

Figure 6.2: Vertical velocities at Kenai Peninsula over 1993-1997 relative to the North-American plate (Freymueller et al., 2000). Thin vertical bars show 95% confidence levels.

processes can have different effects on geodetic signals within only a hundred or so kilometres. From the above studies, the following conclusions can be drawn: (i) tide gauge measurements need to be examined to determine whether earthquakes have occurred during the period of observation, (ii) post-seismic deformation can occur for decades after a significant earthquake, and (iii) uplift rates resulting from tectonic activity can be significantly higher than the effect caused by recent mountain deglaciation. The effect of tectonic activity on geodetic signals can be observed worldwide, for example in the Himalayas, Patagonia, Iceland, California, and the Mediterranean region and these are also areas of mountain glaciation. In conclusion, observed geodetic variations in such tectonically active regions must be examined with caution if the various processes contributing to the signal are to be understood and separated. Moreover, in light of the large displacements caused by tectonic activity, tide gauge measurements in these regions should not be used in studies of sea level. In contrast, in order to constrain tectonic estimates more accurately, one needs to correct for rates of sea-level rise and land movements due to past and recent melting of continental ice masses. As the glacial signals can be large, it is important to have independent measures of the effect deglaciation has on sea level and land movements.

6.2 Contributions from Greenland and Antarctica

The Antarctic and Greenland ice sheets make up over 99% of the total ice volume around the world (see Figure 2.1 on page 15), with the remaining ice being stored in mountain glaciers. Melting of all ice-masses would result in a global sea-level rise of almost 70 m (IPCC, 2007b). Hence, the Antarctic and Greenland ice sheets are by far the largest sources of potential sea-level rise. Over the last century, it is believed that the volume loss of the two ice sheets from melting and iceberg calving is approximately balanced by the gain from average annual solid precipitation falling onto the ice sheets. Annual snowfall on the ice sheets is estimated to be equivalent to a sea-level change of 6.5 mm year^{-1} (Church et al., 2001), hence a small imbalance between snowfall and melting could contribute considerably to present sea-level rise. According to Lemke et al. (2007), Greenland will loose mass during the 21^{st} century, while Antarctica will probably gain mass. Hence, the combined impact on sea-level rise may be small. However, more recent studies show increased melting from coastal regions on both ice sheets. Along the west

and east coast of Greenland and in at least two locations in Antarctica, velocities of large outlet-glaciers show increased rates[4] within the last decade (e.g. Abdalati et al., 2001; Krabill et al., 2004; Luthcke et al., 2006; Thomas et al., 2004; Zwally et al., 2005). However, it is important to note that present-day observations include not only the response of most recent climate changes but also the response due to past changes (Church et al., 2001).

The balance between net accumulation and ablation of ice is different for the two ice sheets. Antarctica has its own climate with cold conditions even during the summer, so there is little surface melting and the ice sheet mainly looses mass by ice discharge into floating ice shelves (Rignot and Thomas, 2002). This is in contrast to Greenland's climate where melting due to higher summer temperatures accounts for around half of the ice loss.

Estimates of the mass balance of ice sheets can be made from altimetry data (airborne or satellite based) and mass-budget calculations. Additionally, the launch of the GRACE[5] satellite allows us to observe temporal variations in the Earth's gravity field (e.g. Tapley et al., 2004a,b). This permits the change in mass of the ice sheets to be monitored from a different perspective. Compared to airborne or laser altimetry which measure the ice elevations, GRACE directly measures the total mass change of the ice sheets. Moreover, GRACE is also sensitive to solid Earth mass changes, in particular to glacial isostatic adjustment of the crust and mantle (a response to past glacial fluctuations) as well as changes in the atmosphere, ocean, and in continental water storage. However, in contrast to many other satellite missions, GRACE gives nearly complete coverage of the high-latitude regions, up to 89°NS.

No detailed data sets of changes in the Antarctic and Greenland ice sheets (i.e. spatial and temporal distribution of changes) were available for use during this study. Therefore, only a brief discussion based on several other studies is presented below. Each of these studies demonstrates that the determination of the mass balances for the two ice sheets is complex. Consequently, there are a wide range of solutions with therefore large uncertainties available.

[4]Note that this does not necessarily imply a sea-level rise as the ice mainly floats. Additionally, in many cases the thinning is more likely a result of changes in the glacier dynamics, e.g. caused by increased accumulation in higher elevations. Hence, the overall change may be very different.

[5]Gravity Recovery And Climate Experiment; http://www.csr.utexas.edu/grace/

6.2.1 Greenland ice sheet

The IPCC (2001) report concluded that the mass balance of the Greenland ice sheet is equivalent to a global sea-level change of 0.05±0.05 mm year^{-1} over the period from 1910 to 1990. In the most recent IPCC (2007b) report, Lemke et al. (2007) summarized on the basis of various individual studies (some are briefly discussed below) that the contribution to global sea-level rise from the Greenland ice sheet is 0.05±0.12 mm year^{-1} over the period 1961-2003 and 0.21±0.07 mm year^{-1} over the period 1993-2003. Various detailed studies of the mass balance of the Greenland ice sheet based on data from all three techniques (mass-budget calculation, altimetry measurements, and changes in the Earth's gravity field) are available. The most striking result from these studies is that they all show an acceleration in mass loss in recent years (see also Figure 6.4). However, due to the relatively short records, the results do not necessarily represent long-term variations but may also contain changes on decadal and shorter time scales. Below, individual result from airborne laser altimetry data as well as satellite altimetry and gravity missions are briefly summarized.

- The study by Krabill et al. (2004) is based on airborne laser altimetry measurements carried out in the years 1993/94 and resurveyed in 1998/99. A comparison between thinning rates during that 5-year period with rates determined during the more recent period 1997-2003 results in elevation changes shown in Figure 6.3a. The estimated total ice loss from the ice sheet during 1993/94 to 1998/99 is equivalent to a global sea-level rise of 0.15±0.04 mm year^{-1}. For the period from 1997 to 2003, Krabill et al. (2004) determined a net ice loss equivalent to a 0.20±0.03 mm year^{-1} eustatic sea-level rise.

- Johannessen et al. (2005) used altimeter data from ERS-1 and ERS-2 satellites[6] (e.g. Johannessen, 1995) over the period 1992-2003 to derive the changes in surface elevation. They derived an average surface elevation change of +5 cm year^{-1} (corrected for vertical land uplift) over an area of almost 1,400,000 km^2 (compromising most of the Greenland ice sheet). However, Johannessen et al. (2005) noted that an integrated assessment of elevation changes (and hence ice-volume or its equivalent sea-level change) for the whole Greenland ice sheet, including its outlet glaciers, can not be made from these observations alone, because the marginal areas are not measured

[6]European Remote-Sensing satellites; http://earth.esa.int/ers/

completely using ERS-1/ERS-2 altimetry. Therefore, the elevation increase measured with ERS satellites can be offset by the ablation at marginal areas. Furthermore, due to the interannual and decadal variability in changes of the Greenland ice sheet the 11-year long data set is too brief to determine a long-term trend.

- Thomas et al. (2006) compared ICESat[7] (e.g. Zwally et al., 2002) data from the year 2004 with the above airborne laser altimetry data observed in 1993/94 and 1998/99. Their results differ significantly from estimates derived from ERS satellites over almost the same period (Johannessen et al., 2005). In particular, Thomas et al. (2006) determined progressive increase in both high-elevation thickening and low-elevation thinning rates. According to Thomas et al. (2006, p. 2), the differences in the high elevation areas to those derived from the ERS satellites 'may result partly from a combination of errors, different spatial coverage, and temporal variability in snowfall during slightly different time periods. But they may also be caused by increased surface melting in recent warm summers'. Thomas et al. (2006) argued that the smaller estimates of thinning rates in the low elevation regions based on the ERS data may be due to the relatively large beam width of the radar (20 m) and concluded that these might therefore underestimate Greenlands ice loss. However, the comparison (when considering the same period) was based on data from ICESat, which has a laser footprint of ∼60 m and hence may also result in considerable uncertainties in the derived thinning rates. Thomas et al. (2006) concluded that the total loss of mass doubled from 4-50 km^3 $year^{-1}$ w.e. (equivalent to a global sea-level rise of 0.01-0.14 mm $year^{-1}$) between 1993/94 and 1998/99 to 57-105 km^3 $year^{-1}$ w.e. (equivalent to 0.16-0.29 mm $year^{-1}$ global sea-level rise) between 1998/99 and 2004. Their estimate of elevation changes over the period 1998/99 to 2004 is shown in Figure 6.3b.

- Velicogna and Wahr (2005) estimated the change in ice mass of the Greenland ice sheet using GRACE gravity fields over the period 2002-2004. Their result indicates a change in ice mass equivalent to a global sea-level rise of 0.21±0.07 mm $year^{-1}$, which agrees with other studies and techniques (see above).

- Ramillien et al. (2006) estimated the ice-volume loss of the Greenland ice sheet also using GRACE data over the period 2002-2005. They calculated

[7] Ice, Cloud, and land Elevation Satellite; http://icesat.gsfc.nasa.gov/

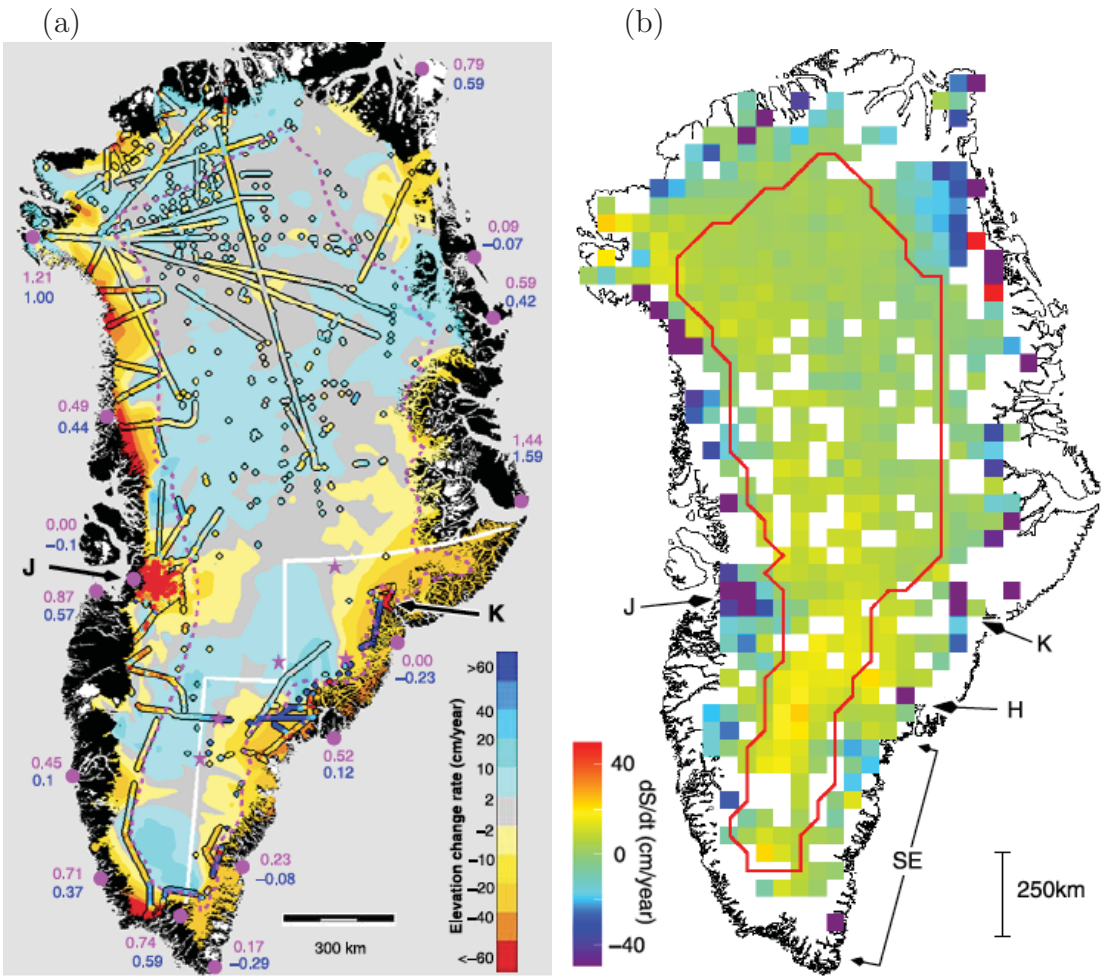

Figure 6.3: Rates of elevation changes in cm year^{-1} of the Greenland ice sheet. (a) Changes over the period 1993/94 to 1998/99 superimposed with changes over the period 1997 to 2003 indicated as the flight lines (Krabill et al., 2004). (b) Elevation changes determined by Thomas et al. (2006) over the period 1998/99 to 2004.

a volume change of -129 ± 15 km^3 year^{-1} w.e., which was corrected for land hydrology contamination and for glacial isostatic adjustment. This ice-volume loss is equivalent to a eustatic sea-level rise of 0.36 ± 0.04 mm year^{-1}.

Both, Krabill et al. (2004) and Thomas et al. (2006), suggest that there is a general increase (or no change) in ice-height of the Greenland ice sheet at higher elevations and a loss in mass at the coastal regions. According to Krabill et al. (2004) the thinning rates at lower elevations could raise sea level by a considerable 0.13 mm year^{-1}. They also note that these thinning rates, derived from laser altimetry measurements, are consistent with other results (summarized in Church et al., 2001) that show increased rates of surface melting during warmer summers and a substantial increase in dynamic thinning.

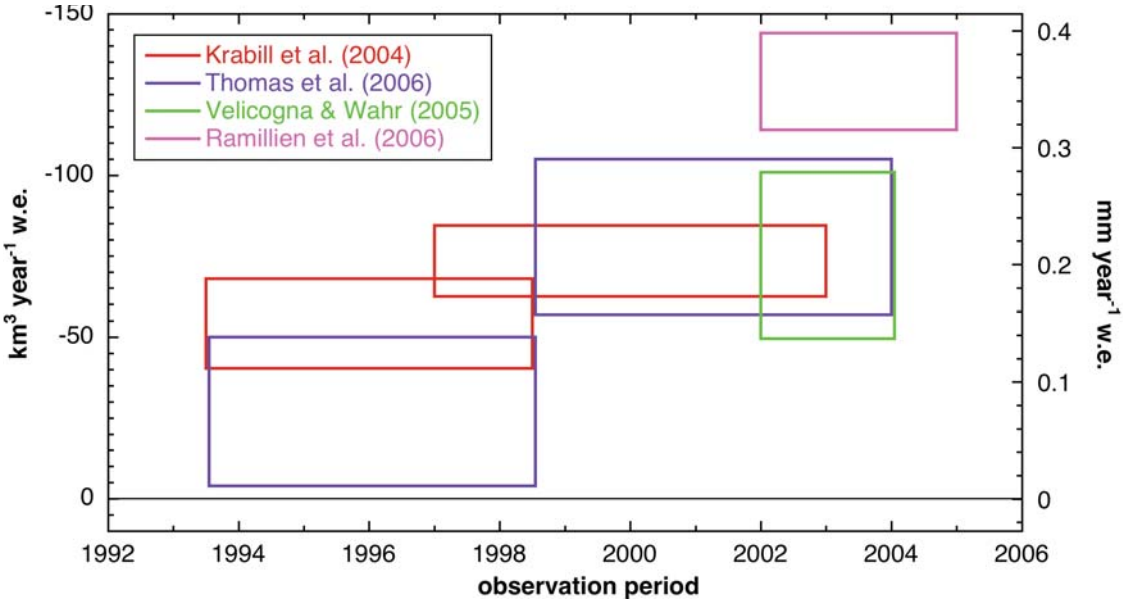

Figure 6.4: Rate of mass change in km^3 year^{-1} w.e. (and in mm year^{-1} global sea-level change) of the Greenland ice sheet derived by Krabill et al. (2004), Thomas et al. (2006), Velicogna and Wahr (2005), and by Ramillien et al. (2006). An acceleration of the mass loss in recent years can be observed.

Differences in results that are based on GRACE data (i.e. Velicogna and Wahr, 2005; Ramillien et al., 2006) are caused by different time intervals considered as well as different analysis methods of the various applied corrections for contamination-effects of gravity signals due to reservoirs other than the ice sheets (i.e. atmosphere, ocean, and terrestrial water reservoirs). Moreover, different geoid solutions due to glacial isostatic adjustment also affect the estimates and explain some of the variations in results.

The mass balance estimates for the entire Greenland ice sheet vary depending on the method used and the period considered (see Figure 6.4). However, most studies agree on an increase in the ice loss during the 1990s up to 2005. Lemke et al. (2007) assessed the available data and techniques and summarised the mass balance of the Greenland ice sheet to

- ➢ -60 to $+25$ km^3 year^{-1} w.e. over the period 1961-2003,
- ➢ -50 to -100 km^3 year^{-1} w.e. over the period 1993-2003,
- ➢ and even higher rates of mass loss between 2003 and 2005.

Furthermore, critical is also the length of observations, such that due to interannual variability of the mass balance, the final estimates vary. Satellite and altimeter data will continue to be recorded over the following years. Thus, observational data (especially from GRACE) available over longer time periods will most certainly

improve the estimates of the present state of the Greenland ice sheet and its continued changes in mass over time.

6.2.2 Antarctic ice sheet

Determining the mass budget for the Antarctic ice sheet is more complex than for the Greenland ice sheet. Antarctica is far larger (12.3 million km^2; Lythe et al., 2001) and more remote than Greenland, and not as well covered by existing geodetic satellites as they don't reach the high latitude areas (e.g. maximum of ∼82°NS for the ERS satellites and 86°NS for ICESat). The Transantarctic Mountains divide the east Antarctic and west Antarctic ice sheets. In contrast to the ice masses in the eastern part which are grounded, the ice sheet over west Antarctica is marine based, meaning that its bed lies below sea-level. This suggests that the west Antarctic ice sheet is more likely to be sensitive to climatic changes, which may result in dynamic responses of the Antarctic ice sheet (e.g. collapse of the Larsen B ice shelf with following acceleration of ice velocities and possible active surging phases of outlet glaciers; De Angelis and Skvarca, 2003).

Four studies estimating recent changes of the Antarctic ice sheet based on altimetry and gravity measurements made from satellites are briefly discussed below.

- The study by Davis et al. (2005) is based on ERS satellite radar altimetry measurements over the period 1992-2003. They determined a thickening rate of 1.8±0.3 cm year^{-1} for east Antarctica and a thinning rate of 0.9±0.3 cm year^{-1} over west Antarctica. These measured elevation changes over the surveyed 7.1 million km^2 of the total ice-sheet area in Antarctica result in an overall thickening rate of 1.4±0.3 cm year^{-1}. The spatial distribution of elevation changes over the period 1992-2003 is shown in Figure 6.5a. Davis et al. (2005) noted that for east Antarctica, the spatial variation in thickening rates matches the snowfall trends. This is in contrast to west Antarctica, where Davis et al. (2005) found that the spatial pattern of the elevation changes is partly correlated with snowfall changes but likely more substantially linked to changes in ice-dynamics. The mean thickening rate of 1.4±0.3 cm year^{-1} derived by Davis et al. (2005), over the observed area of 7.1 million km^2, results in a global sea-level change of -0.12 ± 0.02 mm year^{-1}. However, this study does not include the Antarctic peninsula, steeply sloped coastal regions (the coarse coverage of satellite radar altimetry compromises its utility as a tool to map elevations changes in such regions), and regions

(a)

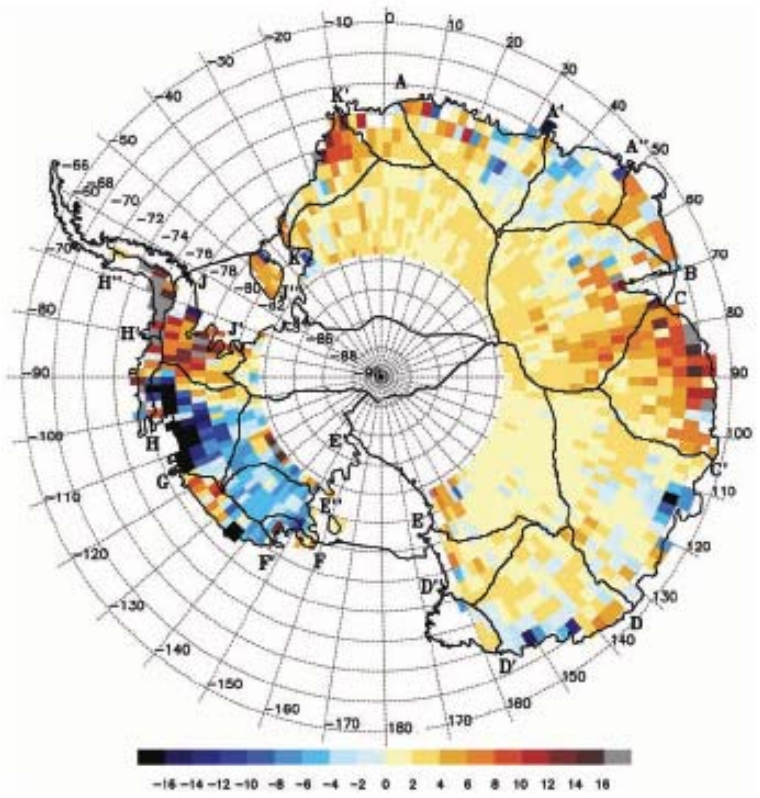

(b)

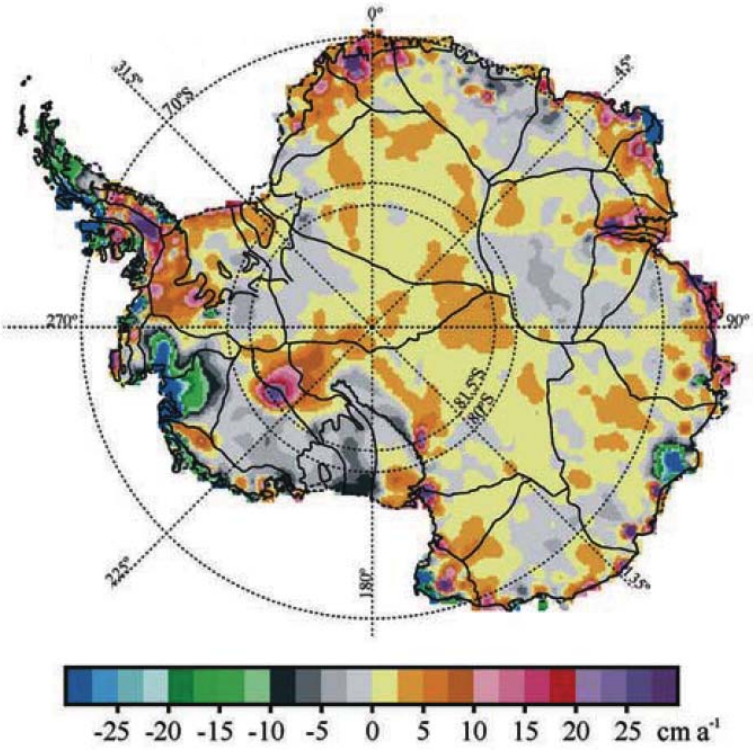

Figure 6.5: Rates of elevation changes in cm year^{-1} of the Antarctic ice sheet (a) from Davis et al. (2005) over the period 1992 to 2003 and (b) from Zwally et al. (2005) over the period 1992-2001.

close to the pole (south of 81.6°S). Hence, the overall contribution to sea-level change could be substantially different.

- Elevation changes determined by Zwally et al. (2005) are based on ERS satellite radar altimetry data over the period 1992-2001. From the observations of over 77% of the Antarctic ice sheet, optimal interpolation procedures were applied in order to provide nearly complete spatial coverage. The resulting elevation changes are shown in Figure 6.5b. Changes in ice thickness are derived by applying a correction for temporal variations in the rate of firn compaction and adjusting for vertical motion of the underlying bedrock. From these ice-thickness changes, estimates of mass changes are determined. Zwally et al. (2005) derived a change in ice mass for west Antarctica of -47 ± 4 km^3 year^{-1} w.e. and $+16\pm11$ km^3 year^{-1}w.e. for east Antarctica. The combined net change of -31 ± 12 km^3 year^{-1} of water is equivalent to a eustatic sea-level rise of 0.08 ± 0.03 mm year^{-1}.

- Velicogna and Wahr (2006) used measurements of time variable gravity from the GRACE satellite over the period 2002-2005 and found that during that period the Antarctic ice sheet lost mass substantially at a rate of 152 ± 80 km^3 year^{-1} (equivalent to a eustatic sea-level rise of 0.4 ± 0.2 mm year^{-1}).

- Ramillien et al. (2006) estimated mass changes over east and west Antarctica of $+67\pm28$ and -107 ± 23 km^3 year^{-1} of water, respectively. These estimates were determined from GRACE data over the period 2002-2005. According to Ramillien et al. (2006), in total, Antarctica was contributing positively to sea-level rise during 2002-2005 at a rate of 0.11 ± 0.09 mm year^{-1}. Ramillien et al. (2006) were unable to clearly identify the reason(s) for the large differences in the total volume changes of the Antarctic ice sheet of their estimates compared to that of Velicogna and Wahr (2006) and attributed it to the different procedures that are applied to correct for glacial isostatic adjustment.

The large error-bars and the discrepancies between the various analyses described above (see also Figure 6.6) demonstrate the difficulty of estimating the ice load history of the Antarctic ice sheet. Nevertheless, all estimates that cover the whole area of the Antarctic ice sheet (all but Davis et al., 2005) are compatible in sign, indicating an overall loss in ice mass. However, more data collection and research is necessary before more accurate estimates can be attained.

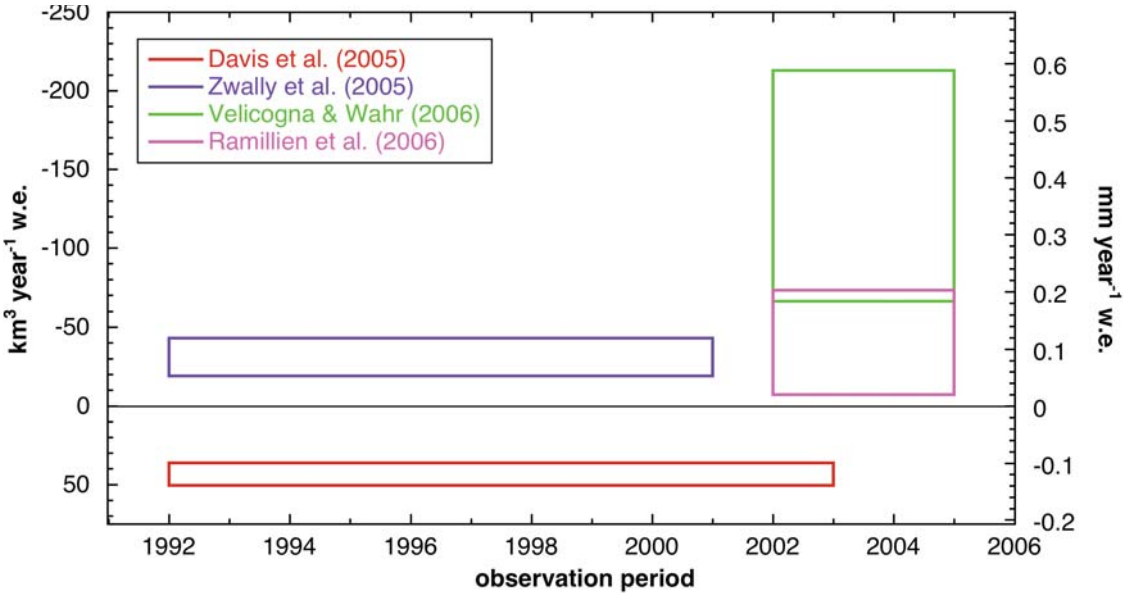

Figure 6.6: Rate of mass change in km^3 $year^{-1}$ w.e. (and in mm $year^{-1}$ global sea-level change) of the Antarctic ice sheet derived by Davis et al. (2005), Zwally et al. (2005), Velicogna and Wahr (2006), and by Ramillien et al. (2006). Note that the mass gain determined by Davis et al. (2005) is derived from data of only about 60% of the total area of the ice sheet and therefore cannot be used as an overall estimate.

6.3 Delayed sea-level response to past ice sheet deglaciation

The term ice age is defined as a period of long-term reduction in temperature of the Earth's climate with ice sheets covering large regions in the northern and southern hemispheres. The occurrence of ice ages are believed to be mainly due to

➢ changes in the characteristics of the Earth's orbit and inclination (Milankovitch cycles; e.g. Hays et al., 1976)

and modulated by several other factors including:

➢ variations in solar output (e.g. Berger, 1978),
➢ changes in the distribution of continents (e.g. Lawver and Gahagan, 2003; Saltzman, 2003), including the change in elevation of continents (e.g. Raymo and Ruddiman, 1992),
➢ eruptions of super-volcanoes (e.g. Humphreys, 1913; Pollack et al., 1976), and
➢ changes in atmospheric composition (e.g. Raymo, 1991; Berner, 1991).

There are three main types of evidence for ice ages: geological, geochemical,

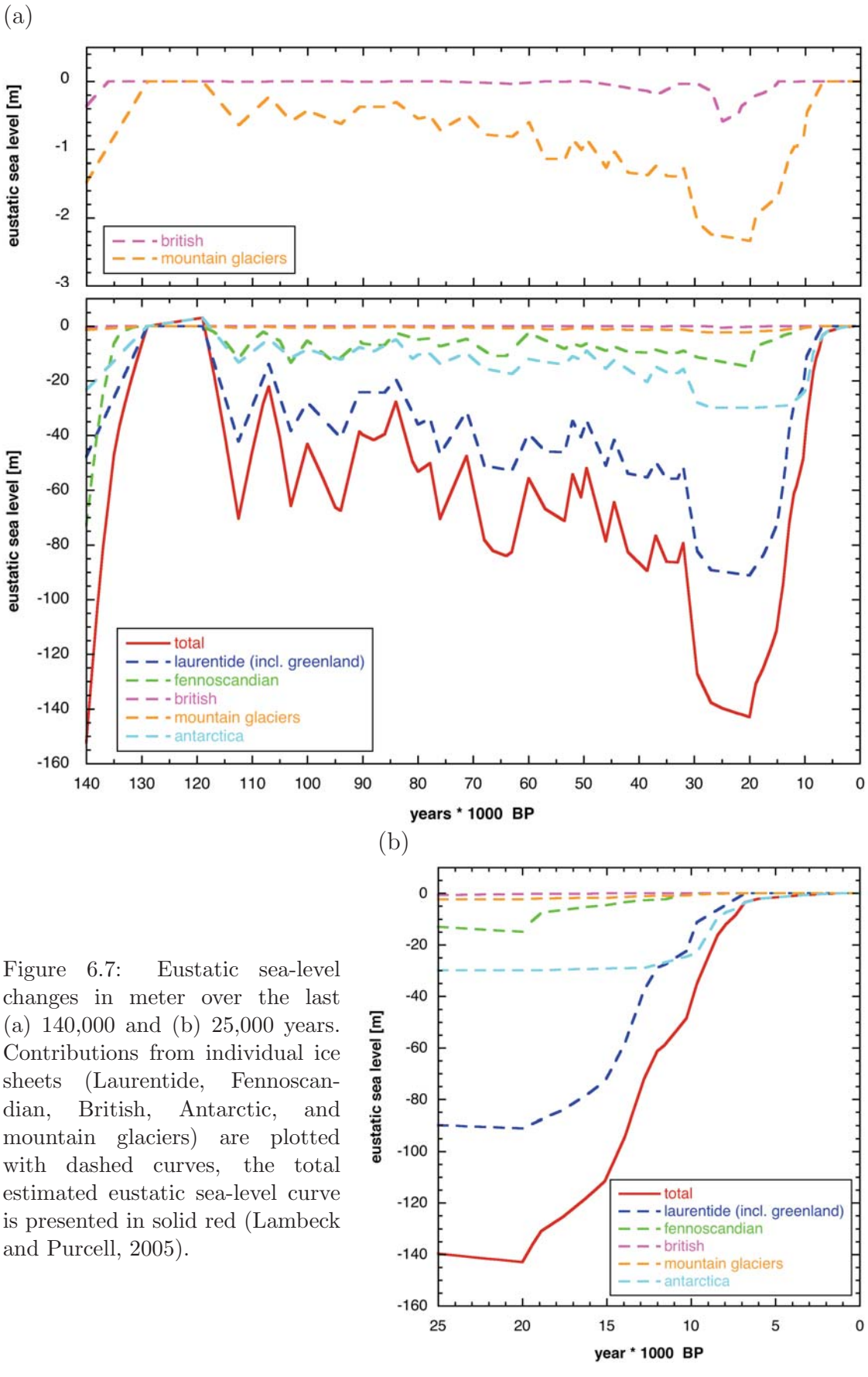

Figure 6.7: Eustatic sea-level changes in meter over the last (a) 140,000 and (b) 25,000 years. Contributions from individual ice sheets (Laurentide, Fennoscandian, British, Antarctic, and mountain glaciers) are plotted with dashed curves, the total estimated eustatic sea-level curve is presented in solid red (Lambeck and Purcell, 2005).

and paleontological. Geological evidence for ice ages includes rock scouring and scratching, glacial moraines, drumlins, valley cutting, and the deposition of till or tillites and glacial erratics in areas presently devoid of glaciers. However, successive glaciations tend to distort and erase the geological evidence of earlier cycles, making it difficult to interpret the earlier records. The chemical evidence for past ice ages mainly consists of variations in the isotopic ratios in sedimentary rocks, ocean sediment cores, and for the most recent glacial periods, ice cores. The paleontological evidence consists of changes in the geographical distribution of fossils.

Within these ice ages, a distinction between colder periods (glacial periods) and warmer periods (interglacial periods) can be made. For example, we are currently in a warm interglacial period with little continental glaciation. The last major glacial period started about 120,000 years ago, reached a maximum about 20,000 years ago (called the *Last Glacial Maximum*, LGM) and ended about 11,000 years ago (see Figure 6.7).

Within the interglacials, again colder and warmer periods occur. One of these warmer periods is the so-called *medieval warm period* which lasted from about the 8^{th} to about the 14^{th} century. This warm period was followed by a colder period with glacial advances called the *Little Ice Age* (LIA) which lasted until around the 19^{th} century. The periods of the LGM and of the LIA and the associated sea-level signal predicted are discussed in more detail in the following sections.

6.3.1 The Last Glacial Maximum (LGM)

The LGM refers to the time of maximum extent of ice cover during the last glaciation, approximately 20,000 years ago. At this time, all of northern Europe and almost all of Canada was covered by huge ice sheets up to 3 km thick (Clark and Mix, 2002; Dyke et al., 2002). Most of the British Isles were covered with ice (Bowen et al., 2002) and the Patagonian ice sheet covered southern Chile to about 41 degrees South (Hulton et al., 2002). On Antarctica and Greenland more ice was stored at the time of the LGM than at present (Anderson et al., 2002; Huybrechts, 2002). Similar, the ice in mountain ranges in Alaska, Himalayas, Europe, and the Russian Arctic covered larger areas than today (e.g. Clague and James, 2002; Owen et al., 2002; Grosswald and Hughes, 2002).

The glaciation/deglaciation history prior to and following the LGM used in the following sections was developed at the ANU. The ice loads are given on

a grid with a spatial resolution of 0.25° in latitude and 0.5° in longitude for the *Laurentide* (covering North America and Greenland) and the *Fennoscandian* (covering northern Europe and the Barents Sea) ice sheets and of 0.5° × 1.0° for the ice covering *mountains* (mainly in Alaska, Patagonia, central Asia, Europe, and the Russian Arctic). The ice cover over Antarctica is given on a 1° grid. More detailed description of these ice sheets is given in Lambeck and Purcell (2005). The estimated eustatic sea-level changes over the past 140,000 and 25,000 years are shown in Figure 6.7, showing the contributions from the individual ice sheets (dashed curves) and the total eustatic sea-level curve (solid red). At the time of the LGM, an ice volume of $\sim 50 \times 10^6$ km^3 of water was stored on continents, which is equivalent to a global sea level that was lower by about 140 m than at present (Figure 6.7b). The biggest contributor to this change was the *Laurentide* ice sheet, followed by the *Antarctic*, *Fennoscandian* ice sheets, the ice covering *mountain glaciers*, and the *British* ice sheet.

Due to the viscoelastic response of the Earth, the effect of the melting of past ice sheets and associated relative sea-level changes and vertical land movements, can be still observed today in tide gauge, GPS, and VLBI measurements. The present-day contribution to geodetic signals due to the deglaciation following the LGM is discussed in the following section with particular focus on two regions, Alaska and Svalbard. The standard Earth model *ma2A* (Section 4.2.1) is used for all following calculations.

6.3.1.1 The LGM in Alaska & Svalbard and its effect on geodetic signals

The extents and heights of the ice loads covering North America (mainly Canada and Alaska) and the Svalbard archipelago at the time of the LGM, 20,000 years ago, are shown in Figure 6.8. By about 7,000 years before present (BP) the Laurentide ice sheet had disappeared. At present, mountains in Alaska are still covered with glaciers, but not to the extent they were at the time of the LGM (see Figure 6.8a). In the ice model, these glaciated areas of Alaska also disappear at around 7,000 BP. In the available ice-load model, Svalbard was completely covered with ice up to a height of approximately 1200 m at the time of the LGM. By about 11,000 BP the ice sheet in this region had completely melted.

Although the distribution of present-day relative sea-level changes due to the glaciation/deglaciation prior to and following the LGM shows a strong spatial variability, many of the tide gauge sites in Alaska are located close to the zero

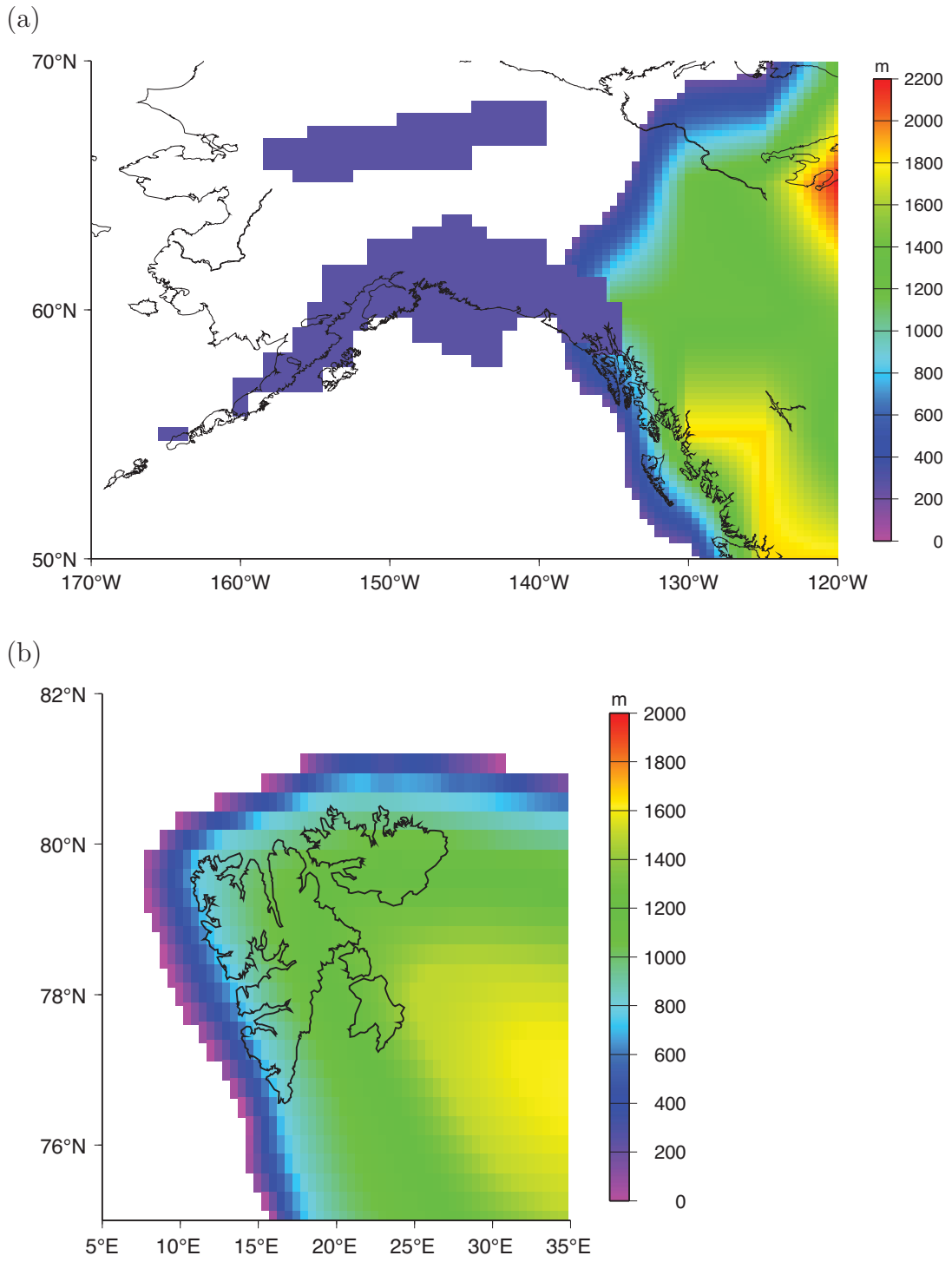

Figure 6.8: Extent and height of ice-cover 20,000 years ago (Lambeck and Purcell, 2005) in (a) Canada and Alaska (Laurentide ice sheet covering Canada, separate ice loads over mountain glaciers in Alaska) and over (b) the Svalbard archipelago (Fennoscandian and Barents ice sheets).

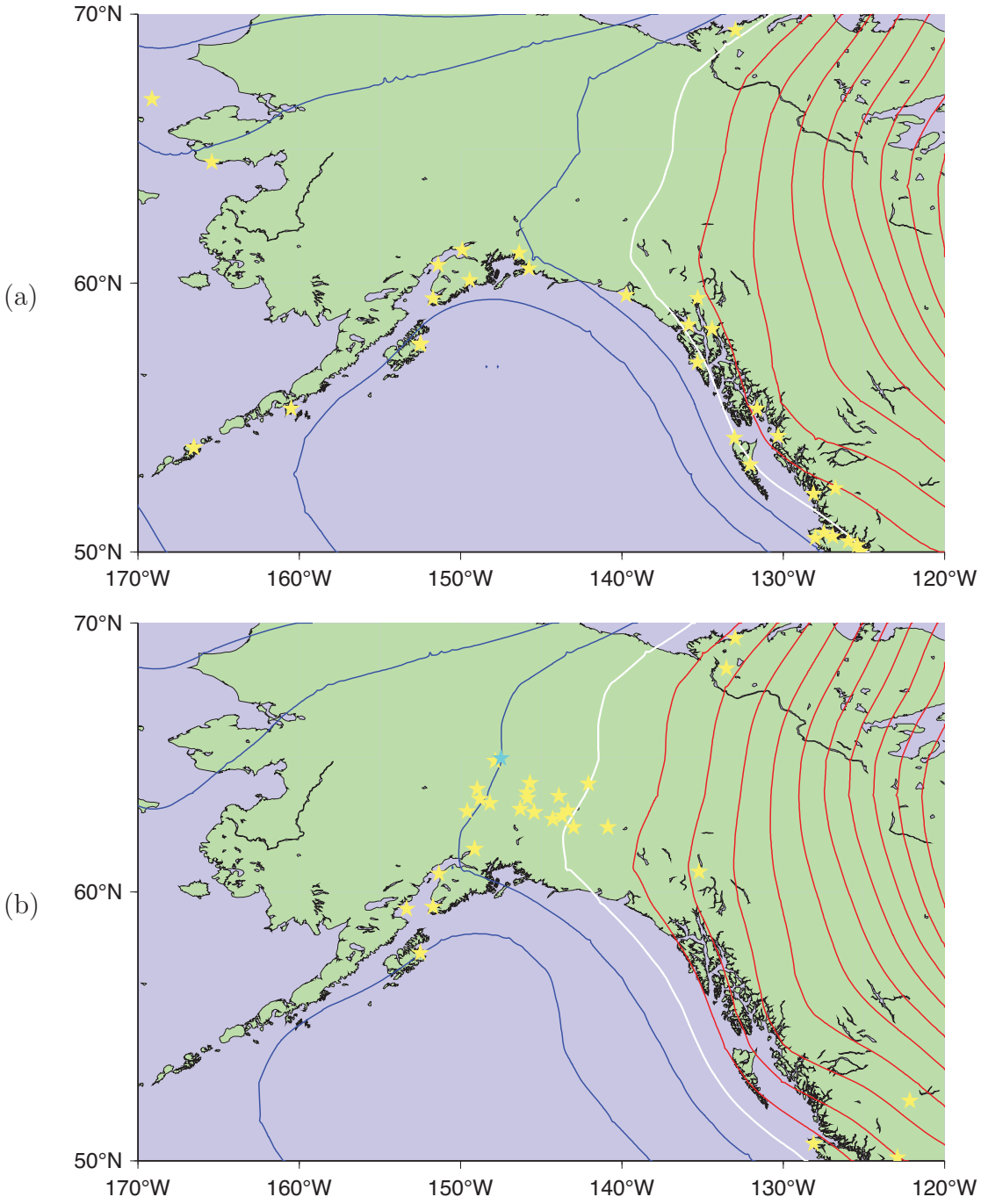

Figure 6.9: Spatial distribution of present geodetic signals in Alaska and Canada due to the deglaciation following the LGM. The contour interval is 0.5 mm year^{-1}. (a) Relative sea-level changes. Red contour lines represent relative sea-level fall, blue contour lines represent relative sea-level rise. White represents the zero contour line (no change). Stars indicate the locations of tide gauge sites. (b) Vertical surface deformation. Red contour lines represent vertical land uplift, blue contour lines represent vertical land subsidence. White represents the zero contour line. Yellow and blue stars indicate the locations of GPS and VLBI sites, respectively.

line (nodeline) and therefore predictions of geodetic signal are small (Figure 6.9a). Relative sea-level rise is predicted for many stations in the western part of Alaska. The same conclusions can be drawn for present vertical surface displacements at geodetic sites in Alaska shown in Figure 6.9b. Many of the GPS and VLBI stations are located close to the zero line, hence the predicted land movements are small.

The spatial distribution of present relative sea-level changes and vertical surface deformation in Svalbard from the on-going rebound of the Earth to past glaciation/deglaciation cycles are shown in Figure 6.10. The same conclusion as above can be drawn for the geodetic sites in Svalbard: predictions of present geodetic signal are small in magnitude as the existing sites in Svalbard are located close to the nodeline of the rebound.

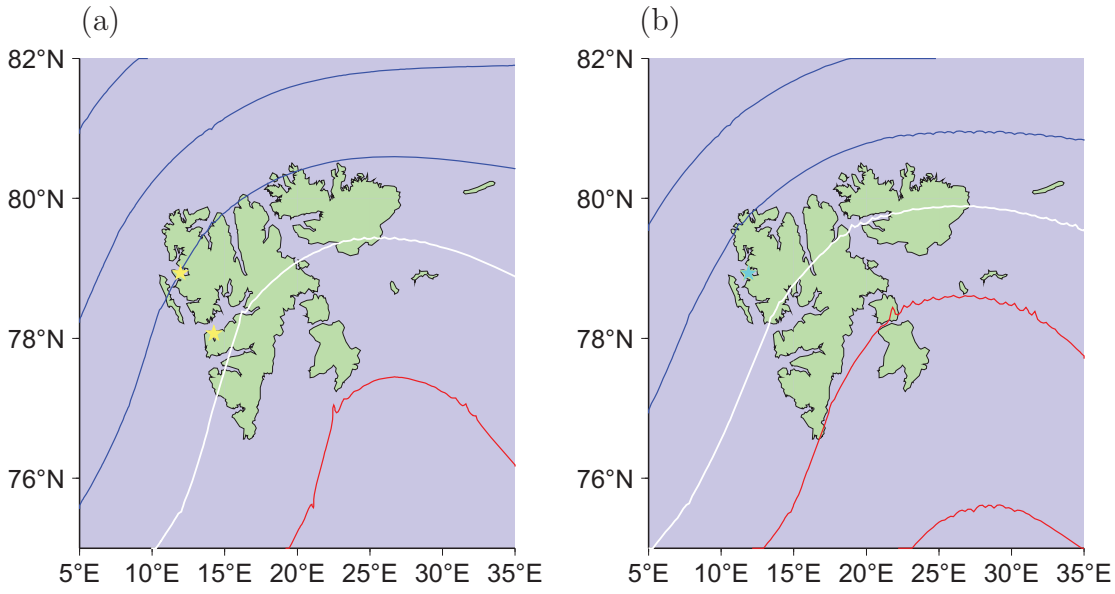

Figure 6.10: Spatial distribution of present geodetic signals in Svalbard due to the deglaciation following the LGM. The contour interval is 0.5 mm year^{-1}. (a) Relative sea-level changes. Red contour lines represent relative sea-level fall, blue contour lines represent relative sea-level rise. White represents the zero contour line (no change). Stars indicate the locations of tide gauge sites. (b) Vertical surface deformation. Red contour lines represent vertical land uplift, blue contour lines represent vertical land subsidence. White represents the zero contour line. The Star indicates the locations of the GPS and VLBI sites.

Figure 6.9a and 6.10a show a pronounced spatial variability in relative sea-level changes due to the deglaciation following the LGM. Therefore, any predictions of geodetic signals are strongly dependent on the location of the site being investigated. Figure 6.11 shows the changes in relative sea level due to the deglaciation following the LGM at the tide gauge sites Cordova and Juneau

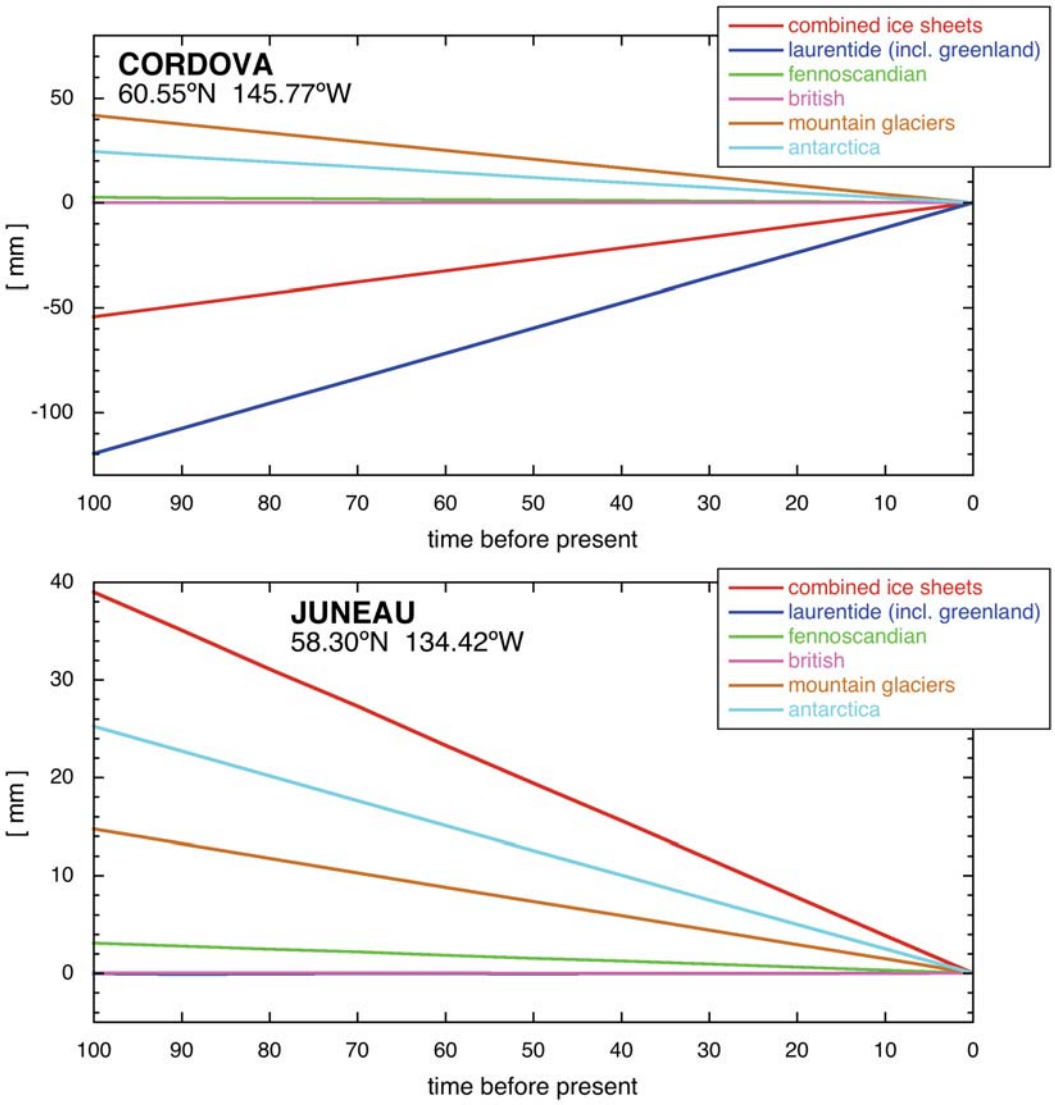

Figure 6.11: Sea level relative to present in mm due to the deglaciation following the LGM at the tide gauge stations Cordova and Juneau (Alaska, see Figure 5.9) over the last 100 years. Contribution to changes in relative sea level caused by the past melting of the Laurentide ice sheet (including Greenland) is shown in dark blue, the Fennoscandian and Barents ice sheets in green, the British ice sheet in pink, the northern & southern hemisphere mountain glaciers in brown, and the Antarctic ice sheet is shown in light blue. Note that at Juneau the contribution to changes in relative sea level from the Laurentide Ice sheet is similar to that of the British ice sheet (blue curve is partly hidden behind the pink curve). The red line represents the total sea-level curve at the site due to melting of all ice covers following the LGM.

(Alaska, see Figure 5.9) for the last 100 years, calculated separately for each of the individual ice sheets (blue, green, pink, brown, and light blue curves) and for a combined solution (red curve). The graph illustrates that the glaciation/deglaciation cycles of the ice cover prior to and since the LGM contribute to present-day relative sea-level changes at these two sites at a rate of $+0.54$ and -0.39 mm year^{-1}, respectively. In other words, 100 years ago sea level is projected to be 54 mm lower at Cordova and 39 mm higher at Juneau than it is now at these sites as a result of the Earth's response to past glaciation/deglaciation cycles. It also shows that every major ice sheet has to be considered, regardless of whether they are located far away or in the vicinity of the observing site, otherwise the signal of the change is inadequately estimated. For example, at these two sites, the contribution from mountain glaciers results in a sea level predicted to be higher 100 years ago than at present. Relative sea level is falling at these sites because of the ongoing uplift of the Earth's surface as a result of past melting from the nearby ice covers. In the case of the Laurentide ice sheet, the contribution to relative sea-level changes at the two sites is very different and even has the opposite sign, indicating that the stations are located on either sides of the nodeline. The contributions from all far field ice sheets (i.e. Fennoscandian, British, and Antarctic ice sheets) are very similar in magnitude for Cordova and Juneau. The sea-level contribution from these ice sheets at the two sites are predicted to be higher 100 years ago than at present. This relative sea-level fall is due to the delayed Earth's response (i.e. subsidence) as a result to the past loading effects due to the melting of the far field ice sheets.

Combined solution for Alaska

As shown above, the delayed sea-level response to past glaciation/deglaciation cycles is significant in parts of the Alaska region. The loading history of past ice sheets (developed at ANU) *and* recent mountain deglaciation are used now to determine associated geodetic signals (denoted *combined solution* below). The latter is based on the numerical model of mountain deglaciation described in Chapter 2 using $\mathrm{T}_{OF}\mathrm{P}_{OFseries}$ (see Section 3.1.4 for more details). The spatial distribution of relative sea-level changes and vertical surface displacements over the period 1961-2000 are shown in Figure 6.12.

Table 6.1 compares estimates of geodetic signals due to the individual contributions (i.e. due to recent mountain deglaciation and due to deglaciation of the past ice sheets) with results of the combined solution at a few tide gauge and GPS sites in

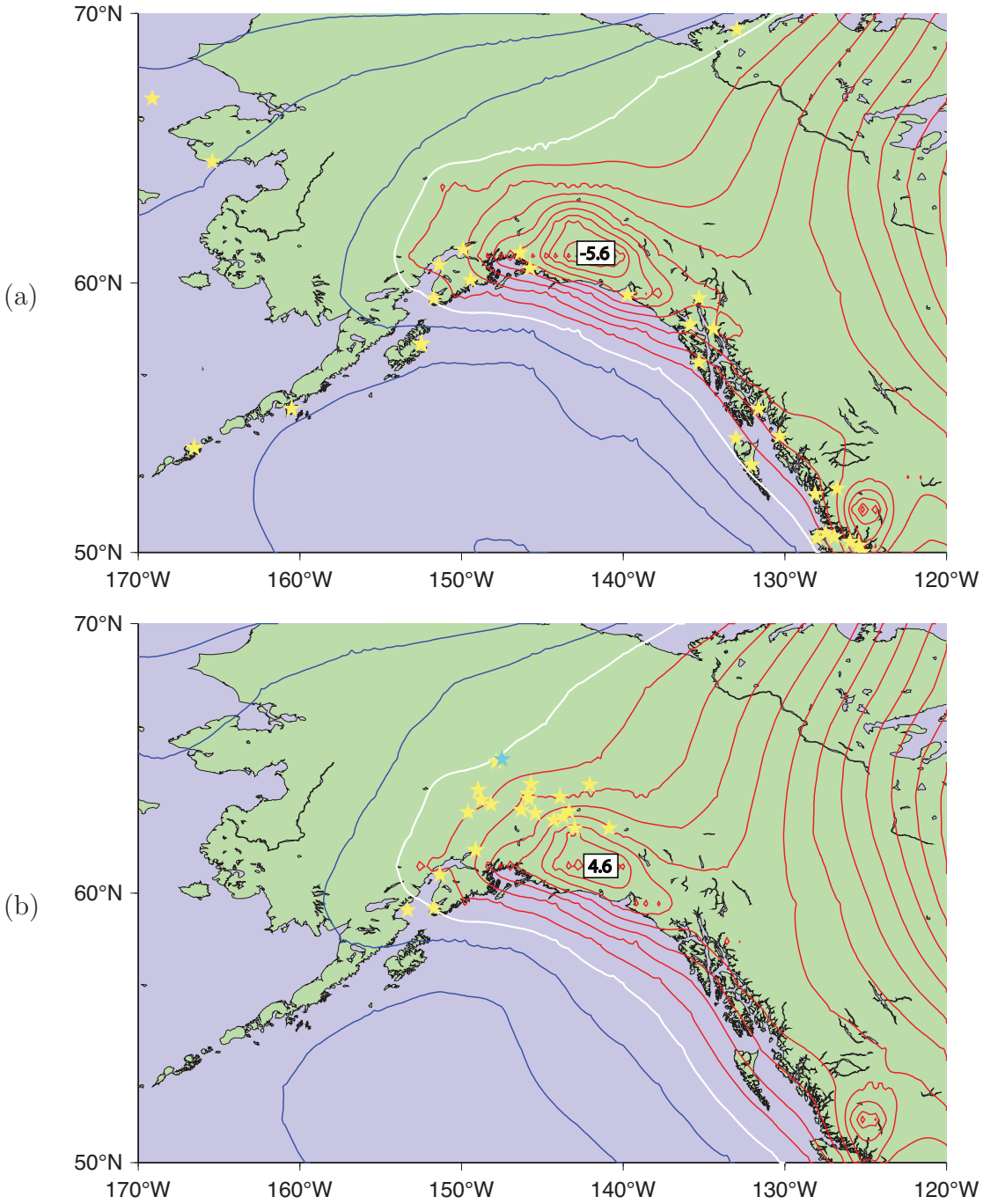

Figure 6.12: Spatial distribution of geodetic signals over the period 1961-2000 in Alaska due to recent mountain deglaciation *and* due to the deglaciation following the LGM. The contour interval is 0.5 mm year^{-1}. Numbers refer to the local maximum rates in mm year^{-1}. (a) Relative sea-level changes. Red contour lines represent relative sea-level fall, blue contour lines represent relative sea-level rise. White represents the zero contour line (no change). Stars indicate the locations of tide gauge sites. (b) Vertical surface deformation. Red contour lines represent vertical land uplift, blue contour lines represent vertical land subsidence. White represents the zero contour line. Stars indicate the locations of GPS (yellow) and VLBI (blue) sites.

	Site	m. gl.	LGM	combined
Tide gauge	**Skagway**	−1.96	−0.45	−2.40
	Yakutat	−3.61	0.22	−3.39
	Juneau	−1.89	−0.39	−2.27
	Sitka	−0.83	0.13	−0.70
	Cordova	−3.02	0.54	−2.49
	Valdez	−4.21	0.46	−3.76
	Anchorage	−1.47	0.60	−0.88
GPS	**Fairbanks** fair	0.47	−0.52	−0.05
	Whitehorse whit	0.87	1.15	2.01
	Palmer atw2	1.44	−0.30	1.14
	Refrigerator Rock frig	2.73	0.09	2.82

Table 6.1: Rates of geodetic signals in mm year^{-1} over the period 1961-2000 at tide gauge and GPS stations in Alaska (see Figure 5.9 and Tables D.1 and D.2 for locations) due to recent mountain deglaciation (*m. gl.*) only, due to the deglaciation following the *LGM* only, and a *combined* solution.

Alaska[8]. The listed estimates indicate that both factors (the deglaciation following the LGM and recent melting of mountain glaciers) can result in signals of the same order and must be taken into consideration when estimating present-day geodetic signals. However, at some sites the effect due to recent mountain deglaciation can be stronger by up to one order of magnitude (e.g. Valdez).

Table 6.1 demonstrates that, at least in principle, it is possible to separate the signals that result from the two different sources. For example for the stations Sitka and Refrigerator Rock, the predicted signal resulting from the past glaciation/deglaciation cycles is very small (the stations are located close to the nodeline) and the signal resulting from recent mountain deglaciation can be isolated and consequently directly compared with the observation. This is, however, only possible in absence of tectonics and any other processes contributing to the geodetic signal at these sites.

Combined solution in Svalbard

Although the Earth's response due to the deglaciation following the LGM at Svalbard's geodetic sites is predicted to be small at present (Figure 6.10), calculations have been undertaken to estimate the geodetic signals resulting from both recent mountain deglaciation (same model as above in the case of Alaska) *and* the deglaciation following the LGM (*combined solution*). The resulting spatial

[8]The stations *fair* and *whit* are part of the IGS network, *atw2* and *frig* are part of the AKDA (Alaska Deformation Array) network. All sites are implemented permanently.

distribution of relative sea-level changes and vertical surface displacements is shown in Figure 6.13. Compared to Figure 6.10, land uplift for almost the whole area of the Svalbard archipelago is now predicted.

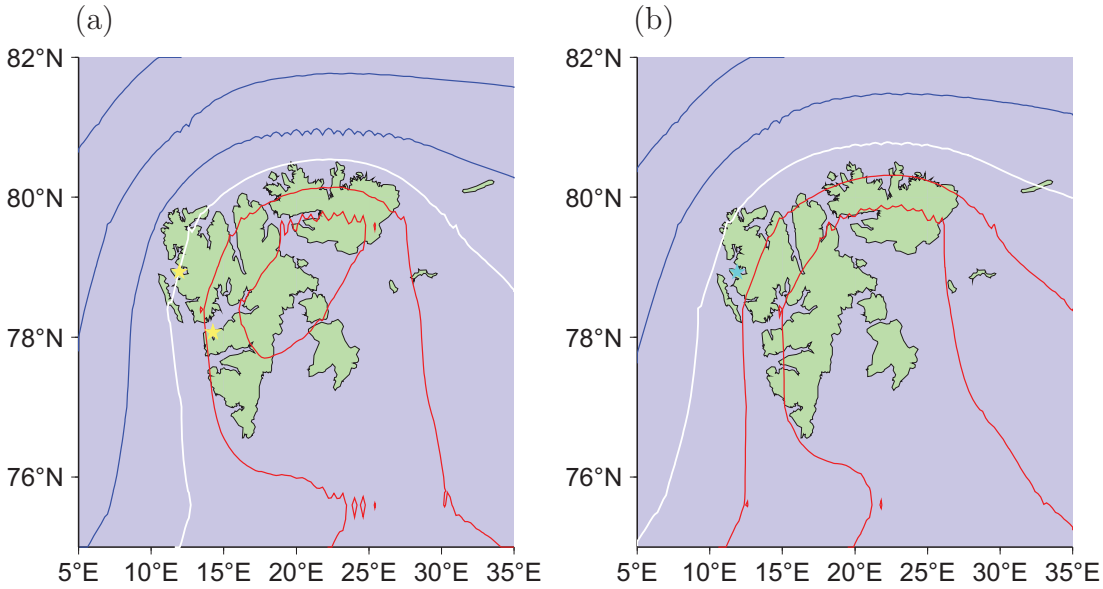

Figure 6.13: Spatial distribution of geodetic signals over the period 1961-2000 in Svalbard due to recent mountain deglaciation *and* due to the deglaciation following the LGM. The contour interval is 0.5 mm year^{-1}. (a) Relative sea-level changes. Red contour lines represent relative sea-level fall, blue contour lines represent relative sea-level rise. White represents the zero contour line (no change). Stars indicate the locations of tide gauge sites. (b) Vertical surface deformation. Red contour lines represent vertical land uplift, blue contour lines represent vertical land subsidence. White represents the zero contour line. The star indicates the locations of the GPS and VLBI sites.

Table 6.2 compares the estimates of relative sea-level changes and surface deformation at existing tide gauge and GPS stations in Svalbard in response to recent mountain deglaciation and to the deglaciation of past ice sheets only. The last column lists the estimates of geodetic signals from the combined solution. Again, it demonstrates that both the deglaciation following the LGM and recent melting of mountain glaciers need to be considered when modelling the present-day geodetic signals. Predictions of geodetic signals in Svalbard as a result from the individual contributions are of the same order, but with opposite signs, which consequently decreases the total signal. At the station Barentsburg, the predicted signal resulting from the deglaciation following the LGM is very small, and hence the overall signal is dominated by the effect recent mountain deglaciation has at this site.

Site	m. gl.	LGM	combined
Barentsburg (tide gauge)	−0.67	0.07	−0.60
Ny Ålesund (tide gauge)	−1.04	0.44	−0.59
Ny Ålesund (GPS & VLBI)	1.00	−0.24	0.76

Table 6.2: Rates of geodetic signals in mm year^{-1} over the period 1961-2000 at the tide gauge and GPS stations in Svalbard due to recent mountain deglaciation (*m. gl.*) only, due to the deglaciation following the *LGM* only, and a *combined* solution.

6.3.2 The Little Ice Age (LIA)

The LIA refers to a period of cooling (including significant glacial advances) that ended the medieval warm period in the 14^{th} century (Grove, 2004). The definition of the start and the end of the LIA is unclear. Suggested causes of the LIA include a decrease in solar activity, an increase in volcanic activity, and variability of the North Atlantic Oscillation mode and the Gulf stream. Evidence indicates that in Europe there have actually been three climatic minima, beginning ∼1650, ∼1770, and 1850, each separated by a slight warming interval. There is evidence that the LIA was a global phenomenon, however the precise timing and nature of these variations are highly variable from region to region (Mann, 2002). For example, while the 17^{th} century was a cold century in Europe, North America does not appear to have experienced unusually cold temperatures. In contrast, as Europe recovered from the colder conditions in the 19^{th} century, North America experienced some of its coldest temperatures (Mann, 2002).

Various studies (e.g. Larsen et al., 2004) suggest that the deglaciation following the LIA still has a significant effect on the present-day geodetic signals in Glacier Bay, Alaska. Wiles et al. (1999) studied tree-ring dates of moraines at 13 glaciers in Alaska in order to assess the glacial fluctuations during the LIA. They concluded that the latest LIA advance took place in the late 19^{th} century. This study has been updated by Calkin et al. (2001) showing that three major intervals of Little Ice Age advances occurred in Alaska, the first one around the middle of the 13^{th} century followed by the second advance from the early 16^{th} century to the middle 17^{th} century. The latest one in Alaska occurred in the last half of the 19^{th} century.

Dowdeswell et al. (1995) suggested that the end of the LIA in Svalbard was marked by an abrupt increase in mean annual air temperature of up to 5 K from the beginning of instrumental observations in 1911 to around 1920. Ziaja (2004) noted that the final cold phase of the LIA in Svalbard occurred in the 1890s.

Given these results, the present geodetic observations in Alaska and Svalbard may still contain a significant signal resulting from the deglaciation following the LIA. The spatial and temporal loading histories of the ice cover following the LIA that are required to calculate geodetic signals were not available, hence no adequate modelling of estimates for geodetic signals were possible here. However, more discussion of some studies dealing with this issue are given in Sections 7.2.4, 7.2.5, and 7.3.2.

6.4 Changes in terrestrial water storage

Besides the storage of continental water in ice sheets and glaciers, water is also stored in *surface water* (including rivers, lakes, and artificial reservoirs) and *subsurface water* (including soil water and ground water). Changes in terrestrial water storage are caused by several factors including:

- climate variations (natural and anthropogenic causes)
  - ➢ cool and wet conditions drive the storage upwards
  - ➢ warm and dry conditions drive the storage downwards
- major human activities that directly affect storage
  - ➢ removal of groundwater from storage by pumping
  - ➢ creation of artificial water reservoirs by constructing dams on rivers
  - ➢ irrigation of cropland
- anthropogenic changes of the physical characteristics of the land surface
  - ➢ urbanization
  - ➢ agriculture
  - ➢ forest harvesting and forest re-growth

It is possible to determine the contribution with medium to high confidence of only a few of the processes listed above. For example, Gornitz (2001) established that between 11% and 13% of the global total annual river runoff is presently stored behind large dams. This impoundment of water in reservoirs and losses due to infiltration and evapotranspiration from artificial lakes and irrigation could prevent the equivalent of 1.3 to 1.7 mm year^{-1} sea-level rise from reaching the ocean (assuming the majority of dams was created in the 1950s and the reservoir capacity was and is still growing at a linear rate). A recent study by Chao et al. (2008) estimated that the water impoundment in world's artificial reservoirs (of almost 30,000 reservoirs) reduced the rise in global sea level by 0.55 mm year^{-1} during the

past half century. However, other processes like groundwater mining, deforestation, and urbanization have a positive effect on global sea-level change. These effects are estimated to contribute 0.4 to 0.8 mm year^{-1} to global sea-level rise. Gornitz (2001) noted that the estimate of the present storage of water on continents by human manipulation of -0.9 ± 0.5 mm year^{-1} w.e. cannot be extrapolated far into the future. Amongst other reasons this is that the rate of dam-building is likely to decrease and deforestation may also decrease.

Some of the factors listed above are likely to make a large contribution to sea-level change. However, many of them are very difficult to model, especially with respect to projected future trends. Attempts to quantify those changes in terrestrial water storage have been undertaken at several institutions. Results of those models are, amongst other sources, available from the GGFC Special Bureau of Hydrology website[9]. As an example, the global spatial distributions of the annual mean changes in terrestrial water storage of the LDAS[10] surface model developed at the Climate Prediction Center (CPC) is shown in Figure 6.14a. This data set (Fan and den Dool, 2004) is forced by observed annual precipitation, the surface radiation budget, surface pressure, humidity, 2-m temperature, and horizontal wind speed from the NCEP[11] reanalysis. The output represents soil temperature and soil moisture in four layers below the ground. At the surface it includes all components affecting energy and water mass balance, including snow cover, depth, and albedo. It is given on a half degree grid over the period 1980-2006 on a monthly base. This data set has been used in this thesis to calculate the spatial distribution of linear trends over the 27-year period and the result is shown in Figure 6.14b.

Globally, the water stored on continents (excluding Antarctica) in the CPC model is on average 20 cm of equivalent average water height (expressed in equivalent sea-level change this corresponds to -117 mm). Figure 6.15a shows the area-weighted inter-annual changes in global terrestrial water storage. Over the period 1980-2006 the global storage shows a small negative trend -27.57 km^3 year^{-1} of water (equivalent to 0.076 mm year^{-1} global sea-level rise). The average change over the period from 1981 to 1998 of 0.30 mm year^{-1} w.e. is almost three times the result of Milly et al. (2003) based on the Land Dynamics (LaD) model of Milly and Shamkin (2002). In contrast, over the period 1993-1998, the average change of 0.12 mm year^{-1} w.e. in the CPC model is only half that derived by Milly et al. (2003) over the same period. Locally, the trends of the CPC model can vary

[9] Global Geophysics Fluid Centre; http://www.csr.utexas.edu/research/ggfc/dataresources.html
[10] Land Data Assimilation System
[11] National Centers for Environmental Prediction; http://www.ncep.noaa.gov/

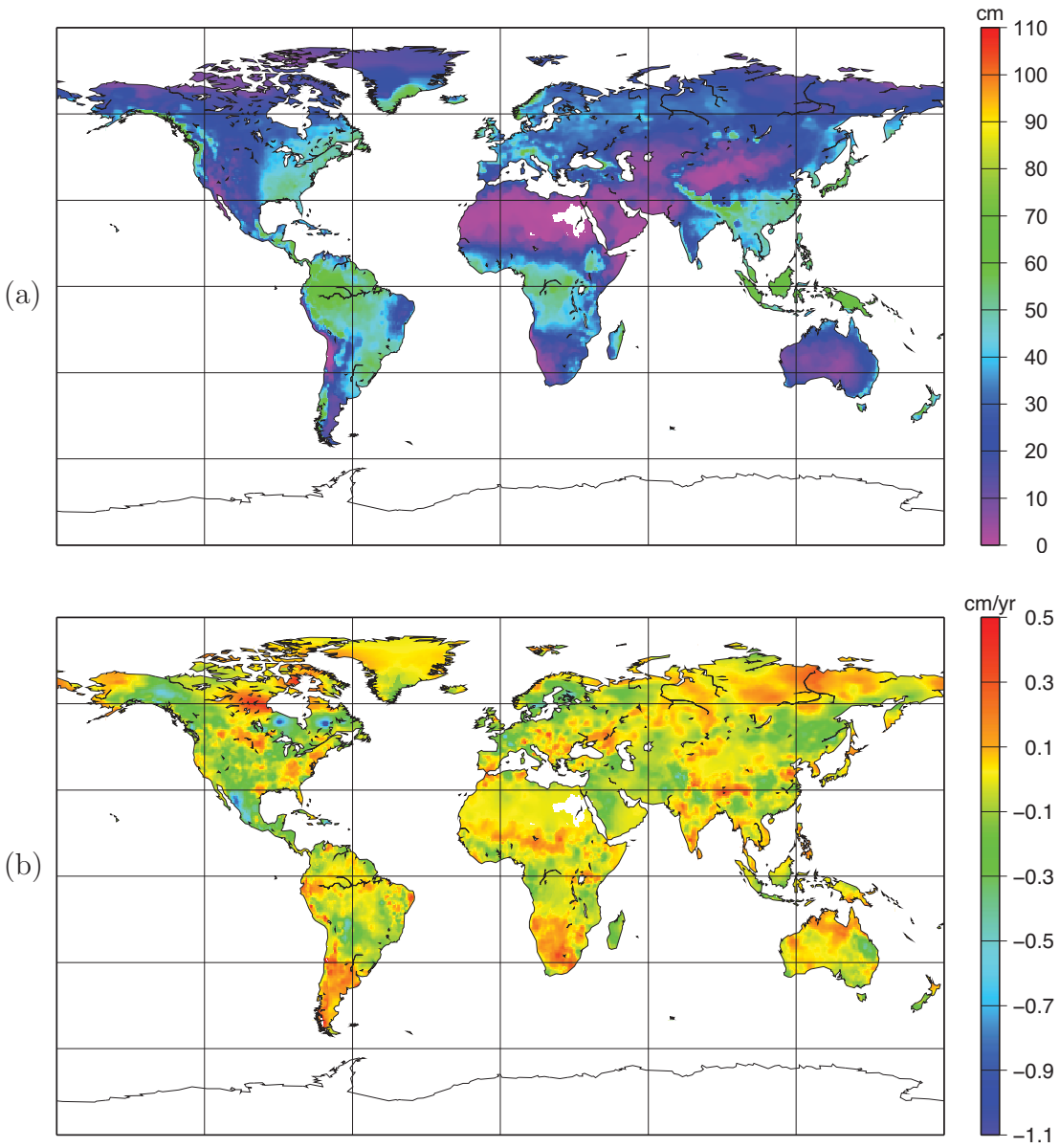

Figure 6.14: (a) Mean annual signal in cm and (b) linear trend of changes in cm year^{-1} of terrestrial water storage of the CPC model given on a 0.5° × 0.5° grid over the period 1980-2006.

considerable (see Figure 6.14b), mostly between approximately −1.1 and +0.5 cm of equivalent water height.

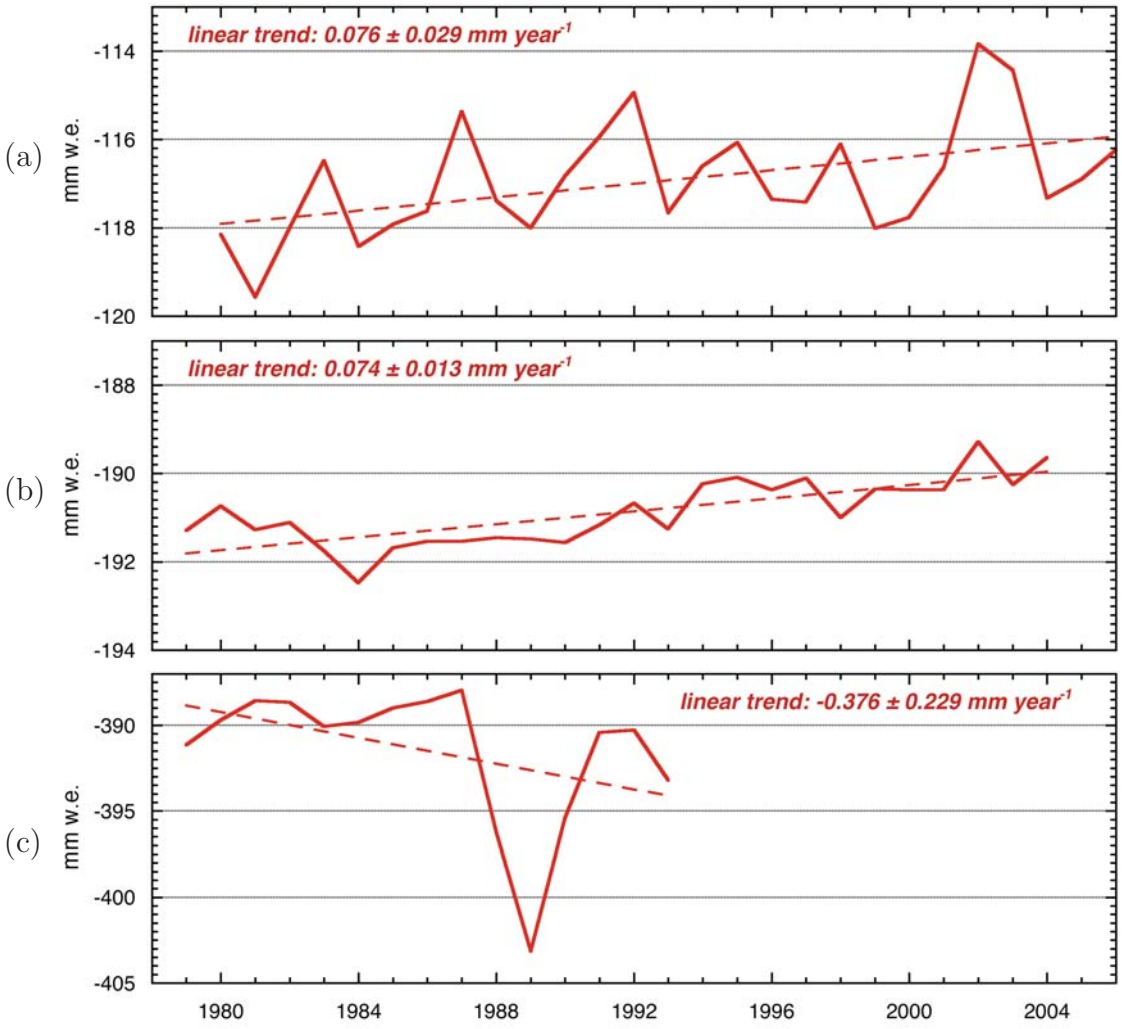

Figure 6.15: Effect on global sea level in mm w.e. derived from changes in terrestrial water storage of the (a) CPC data set over the period 1980-2006, (b) NCEP data set over the period 1979-2004, and (c) ECMWF data set over the period 1979-1993.

Comparing different data sets of terrestrial water storage that are available (e.g. those from the Special Bureau of Hydrology website) show a large degree of variability in the spatial distribution of continental water. This concerns both magnitudes and trends of terrestrial water storage (see Figure 6.15b and 6.15c)[12]. This also complements the estimate by Church et al. (2001) who reviewed all available literature and concluded that between −1.1 and +0.4 mm year^{-1} of global sea-level change comes from changes in terrestrial water storage. This considerable spread demonstrates the large uncertainties that exist. Consequently, the latest

[12]details on these data sets (NCEP and ECMWF) are not given here but can be obtained from the GGFC webpage: http://www.csr.utexas.edu/research/ggfc/dataresources.html

IPCC (2007b) report even omitted the contribution from terrestrial water storage from the estimated sea-level budget as it is so poorly known.

Due to the isostatic rebound and geoid changes to variations in terrestrial water storage, variability in local sea level can also be predicted. The spatial and temporal variations in terrestrial water storage determined from the CPC data set are used to calculate the corresponding relative sea-level changes, shown in Figure 6.16. It illustrates that, where positive trends in storage are computed (e.g. in South Africa and Patagonia) relative sea level is rising and for negative trends in storage the response of sea level is a relative fall (similar to the sea-level response to mountain deglaciation). Overall, relative sea-level changes in this model are small, i.e. variations over the entire period do not exceed approximately ± 0.3 mm year^{-1}.

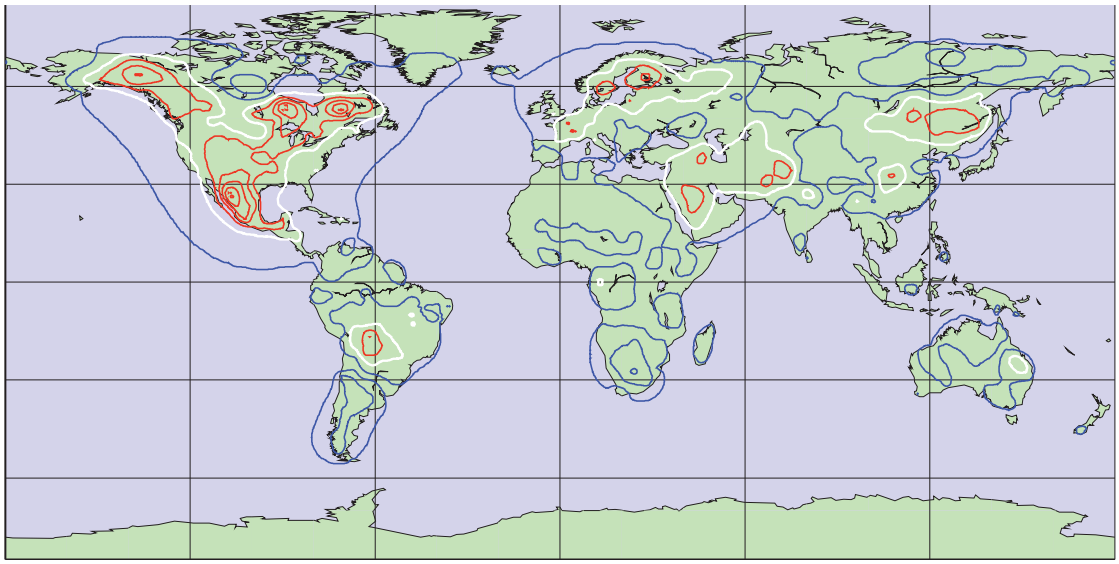

Figure 6.16: Spatial distribution of relative sea-level changes due to variations in terrestrial water storage of the CPC data set over the period 1980-2006. Red contour lines represent relative sea-level fall, blue contour lines represent relative sea-level rise. White represent the zero contour line (no change). The contour interval is 0.05 mm year^{-1}.

Another way of estimating the changes in terrestrial global water storage is using observations of the GRACE satellite, as has been undertaken by Ramillien et al. (2008) over a 3-year time span. Their results indicate large negative trends in river drainage, in particular in the Amazon, Ganges, Mississippi, Nile, Parana, and Zambezi basins. In contrast, their calculated positive trends in other areas are small. The total of 27 river basins studied in Ramillien et al. (2008) contribute $+0.19 \pm 0.06$ mm year^{-1} to global sea-level change. However, they note that these trends are not likely to be representative for long-term variations but are likely to

be linked to inter-annual variability. Hence, much longer observational time series are required to determine long term-trends more accurately.

6.5 Thermal expansion of the ocean waters

Thermosteric sea level is defined as the variation in sea-surface height caused by expansion or contraction of ocean volume due to temperature changes. Various studies on regional scales (summarised in the IPCC, 2001, report) show that there are widespread indications of thermal expansion of the order of 1 mm year^{-1} over the 20^{th} century. Estimates of global ocean thermal expansion over the last century range from 0.3 to 0.7 mm year^{-1} and from 0.6 to 1.1 mm year^{-1} over recent decades (Church et al., 2001). The IPCC (2007b) report concluded that thermal expansion contributed 0.42±0.12 and 1.6±0.5 mm year^{-1} to global sea-level rise over the periods 1961-2003 and 1993-2003, respectively.

Studies of the ocean heat content over the last few decades indicate strong spatial variability. For example, Levitus et al. (2000) used all available historical oceanographic observations to estimate changes in heat content. They concluded that prior to the mid 1970s, the upper 300 m of the Pacific, Atlantic, and Indian Ocean basins were cooler than from the mid 1970s until present. Regarding the heat content to a depth of 3000 m, temperatures were also cooler before the 1970s than after. Nevertheless, the warming in the Pacific and Atlantic started earlier in the 1950s.

In situ temperature observations for the period 1955-2003 studied by Antonov et al. (2005) show a linear trend in global thermal expansion of 0.40±0.05 mm year^{-1} for the 0-3000 m layer. The 0-700 m layer accounts for most of this estimated change (0.33±0.04 mm year^{-1}). However, the true picture is more complicated. The time series of thermosteric sea-level change shows substantial inter-decadal variability, and changes in thermosteric sea level are geographically variable. In particular, whereas strong warming is found around 40°N in the Atlantic, the Pacific has a significant negative trend (Antonov et al., 2005). Furthermore, significant negative trends are also found in the North-Atlantic and in the subtropical/subpolar transition zone of the North-Pacific. In addition to the trends over the period 1955-2003, Antonov et al. (2005) also analysed changes in ocean heat content over the period from 1993 to 2003 and concluded that the trends for the latter period are more than three times larger (1.23±0.2 mm year^{-1}) than for the entire

period. This result is supported by the slightly higher value of 1.6±0.3 mm year^{-1} of thermosteric sea-level rise over the period 1993-2003 estimated by Willis (2004) (using oceanographic observations together with satellite altimetry). Antonov et al. (2005) noted that a similar rate of global thermosteric sea-level rise occurred from the late 1960s to the mid 1970s. The largest contribution to global thermosteric sea-level rise over 1955-2003 came from the Atlantic. However, the Pacific was responsible for the majority of thermosteric sea-level rise over the period 1993-2003 (Antonov et al., 2005).

Lyman et al. (2006) found a rapid decrease in globally integrated upper (0-750 m) ocean heat content anomalies between 2003 and 2005 using primarily ARGO[13] measurements. However, they had to correct this statement of global cooling as they found that it is an artefact resulting from the combination of two different instrumental biases (Willis et al., 2007). This study illustrates that considerable problems of estimating the ocean heat content anomalies correctly can occur due to the problems of quality control and of potential biases among different instrumental types.

Another study of thermosteric sea-level changes over the period 1955-2003 has been undertaken by Ishii et al. (2006). Their computation of steric sea level is based on temperature analyses and has been verified with tide gauge observations and TOPEX/Poseidon sea-surface height data. They estimated a contribution to global sea-level change of 0.31±0.07 mm year^{-1} due to the thermosteric component. These studies demonstrate that additional to the annual and interannual variability in thermosteric sea-level changes, there is also a significant spatial variability in their regional trends.

6.5.1 Relative sea-level changes due to ocean bottom pressure changes caused by thermal expansion

As discussed in the previous section, ocean thermal expansion does not alter the total global ocean mass but can nevertheless result in relative sea-level changes. The heat uptake by the ocean (in case of a warming climate) varies locally both horizontally and in depth. In a simplified model the total water column in the deep ocean tends to expand more than in shallow areas (illustrated with arrow ① in Figure 6.17). In order to maintain an equipotential surface, water has to flow

[13]ARGO is a global array of ∼3,000 free-drifting floats that measures the temperature and salinity of the upper 2000 m of the ocean; http://www.argo.net/

from the deep ocean to the shallow areas. This redistribution of water (illustrated with arrows ② in Figure 6.17) consequently results in a spatial change in ocean bottom pressure. Moreover, these ocean bottom pressure changes result in *second order relative sea-level changes*. The application of this theory is discussed in the remainder of this section.

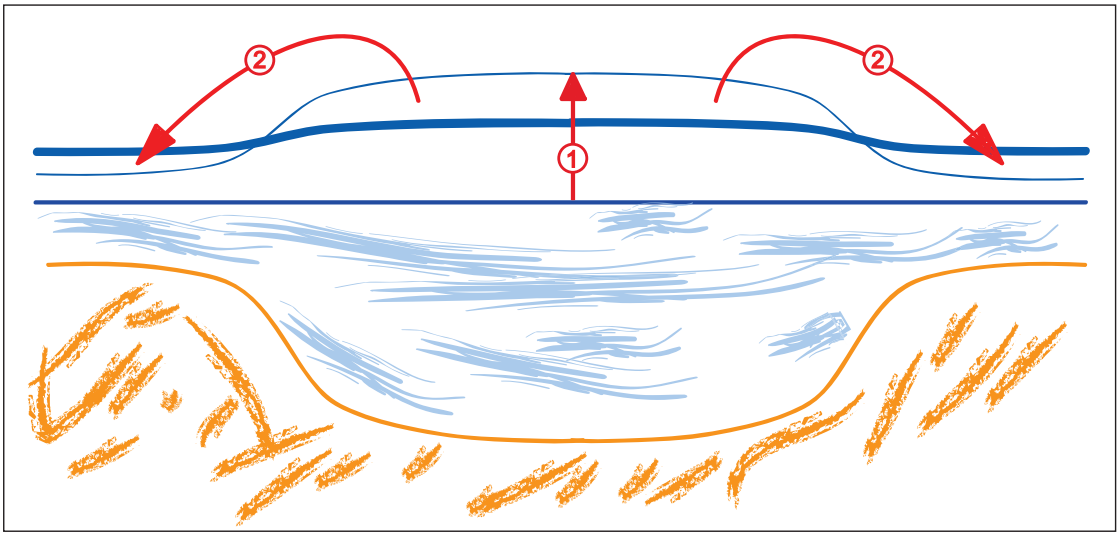

Figure 6.17: Schematic plot of changes in sea-level due to thermal expansion. The arrow ① indicates the change in sea-level due to thermal expansion of the oceans, showing a simple model with greater expansion in deep waters and less expansion in shallow regions. The arrows ② illustrate the flow of water from areas of greater expansion (deep ocean areas) to areas with less expansion (shallow areas). The bold blue line shows the redistributed sea level due to non-uniform thermal expansion. This redistribution of water changes the pressure on the ocean's floor and ultimately also sea level itself.

Atmospheric CO_2 concentrations and projected global sea-level rise over the period from 1860 to 2200 are plotted in Figure 6.18 (adopted from Landerer et al., 2007a, Figure 2). The analyses are based on IPCC scenario simulations. For the period 1860-2000 coupled experiments with transient greenhouse gas concentrations and aerosol forcing from pre-industrial to present-day values were conducted. Simulations for the 21^{st} century are based on the A1B (Nakicenovic et al., 2000)[14] climate scenario of the IPCC (2001) report. From 2101 to 2200 the greenhouse gas concentrations in the simulations are fixed at the 2100 level.

[14]The A1B scenario describes 'a future world of very rapid economic growth and global population that peaks in mid-century and declines thereafter, and the rapid introduction of new and more efficient technologies' (IPCC, 2001, p. 63). The source of energy used to drive the expanding economy in the A1B scenario is a balance between fossil fuels and other energy sources.

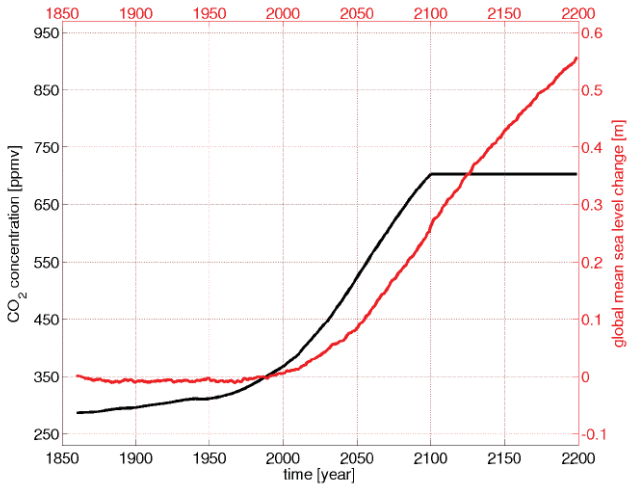

Figure 6.18: Atmospheric CO_2 concentration (black curve) and global mean sea-level rise (red curve) in response to the CO_2 forcing from 1860 to 2200 (Figure 2 in Landerer et al., 2007b).

Landerer et al. (2007a) calculated ocean bottom pressure changes caused by secular oceanic mass redistribution due to thermal expansion. They developed a numerical model for the mass transfer from deep open water to coastal (shallow) areas. A data set of ocean bottom pressure changes has been provided by Felix Landerer[15]. The variations are expressed as changes of mass load in meters of water and are given on an annual basis from 1860 to 2200 on a $1^o \times 1^o$ grid. Three examples of 10-year averages are shown in Figure 6.19 (see Figure E.1 on page 338 for plots over other time periods). The plots show an increase in intensity of the redistribution of mass particularly from 2000 onwards. This corresponds to the curve of the global mean sea-level rise due to thermal expansion in the IPCC A1B emission scenario (Figure 6.18) where mean sea-level rise begins around 2000.

The plots in Figure 6.19 show the overall transfer of mass from the southern to the northern hemisphere. In particular, the Arctic Ocean shelves experience an above-average increase in mass load. It appears that there is a good correlation between ocean bottom pressure changes and ocean bathymetry. For the IPCC scenario simulations used here, positive loads of up to 0.4 m by the end of the 21^{st} century and 0.8 m by the end of the 22^{nd} century are projected mostly for the Arctic Sea, while the deeper oceans (especially in the southern hemisphere) experience negative loads of -0.2 m and -0.4 m by 2100 and 2200, respectively.

The above results represent the redistribution of mass assuming a rigid Earth. Hence, the so-called *second order relative sea-level changes* as a result of the viscoelastic response of the Earth to the redistribution can now be calculated. Since

[15]Felix Landerer is a PhD student at the Max Planck Institute for Meteorology working on sea-level changes in response to climate change, in particular regional effects due to changes in the ocean's general circulation patterns. http://www.mpimet.mpg.de/~landerer.felix

only thermal expansion is considered here, no mass is added or taken away from the ocean and the total change in mass over the oceans is zero. The bottom pressure changes, expressed as water-mass loads, have been implemented in the sea-level program (the *calsea* program, see Section 4.3). As it turned out, using the *calsea* program as it is, is inadequate for solving second order relative sea-level changes due to ocean bottom pressure changes. This is because the loading/unloading appears only over the oceans and the sea-level program treats these loads in the same way as floating sea-ice. When floating sea-ice is added to the ocean in the *calsea* program it is treated as additional water and the load is distributed across the oceans. It does not have a local "point load" effect because the ice is supported hydrostatically. Hence, non-uniform ocean bottom pressure changes are not correctly represented in the *calsea* program as it was not written to address that problem. However, considering only the deformational component including the corresponding geoid changes of the sea-level equation (see Section 4.3), resultant relative sea-level changes can be computed.

Relative sea-level changes due to ocean bottom pressure changes for 10-year averages are shown in Figure 6.20. Changes in relative sea level from this source are negligible until the beginning of the 21^{st} century, which again correlates with the global curve of mean sea-level rise due to thermal expansion in the climate scenario (Figure 6.18). By the end of the 22^{nd} century, relative sea-level rise reaches a maximum of approximately 60 mm in the Arctic. This value is expressed relative to the mean of the period 1860-1869, which is assumed to be an unperturbed period. In addition, as the spatial distribution of relative sea-level changes correlates with the spatial distribution of ocean bottom pressure changes (see Figure 6.19), a rise in second order relative sea level is predicted mostly in coastal areas, in particular in the Arctic Ocean, whereas second order relative sea level falls in deep ocean areas.

Assuming this climate scenario adequately represents future thermal expansion, relative sea-level changes due to the redistribution of water caused by secular ocean mass redistribution are amplified by about 10% by the second order relative sea-level changes due to these ocean bottom pressure changes. While there is a variety of uncertainties in thermal expansion models (e.g. size of the surface warming, the effectiveness of heat uptake by the oceans for a given warming, and the expansion resulting from a given heat uptake; see Section 11.5 in Church et al., 2001), the predicted future sea-level changes will have to be increased by 10% to account for these second order variations in sea level.

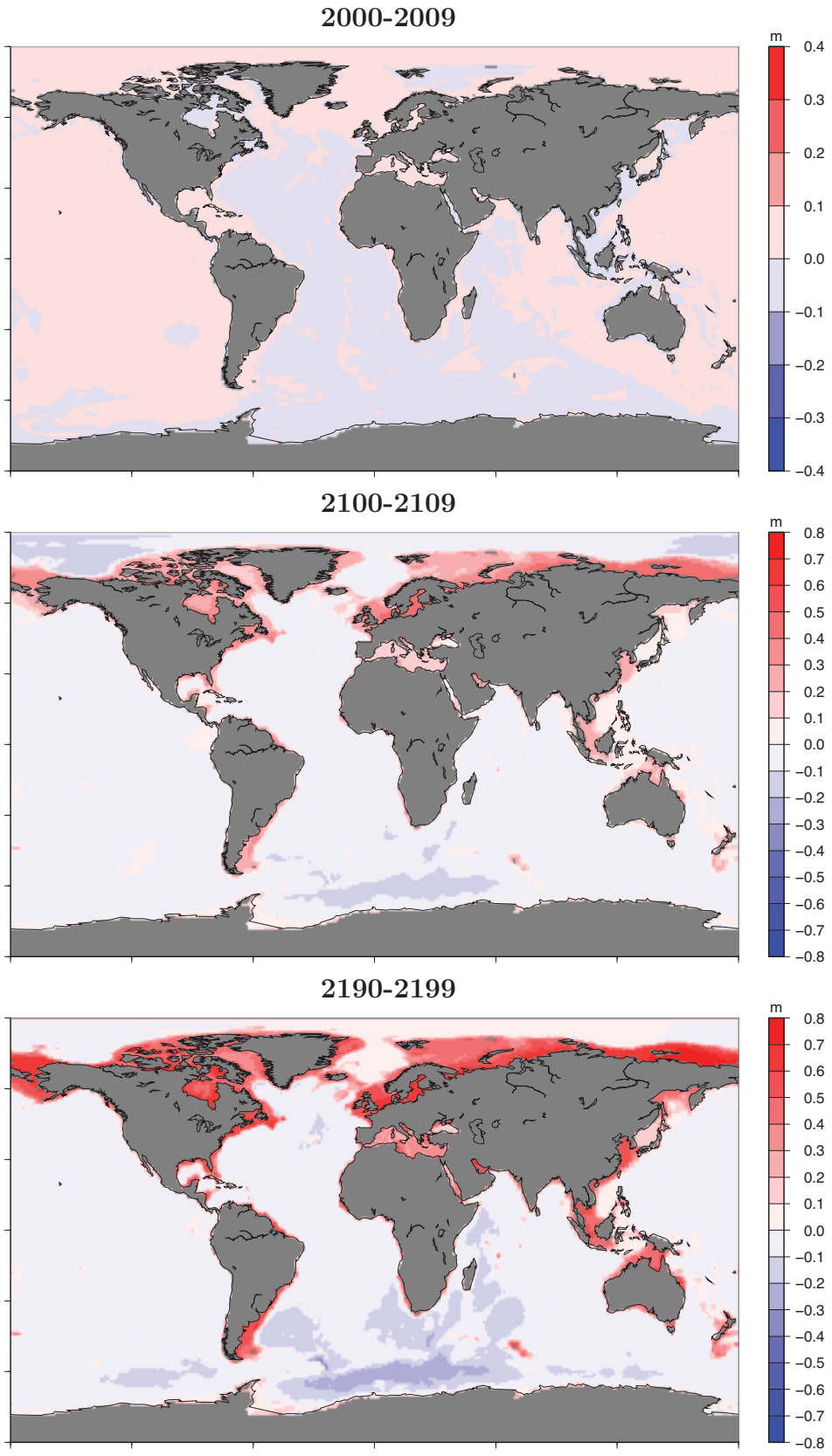

Figure 6.19: Thermal expansion induced ocean bottom pressure changes of 10-year averages relative to an unperturbed ocean expressed in meters of mass load (see Figure E.1 on page 338 for plots over other time periods).

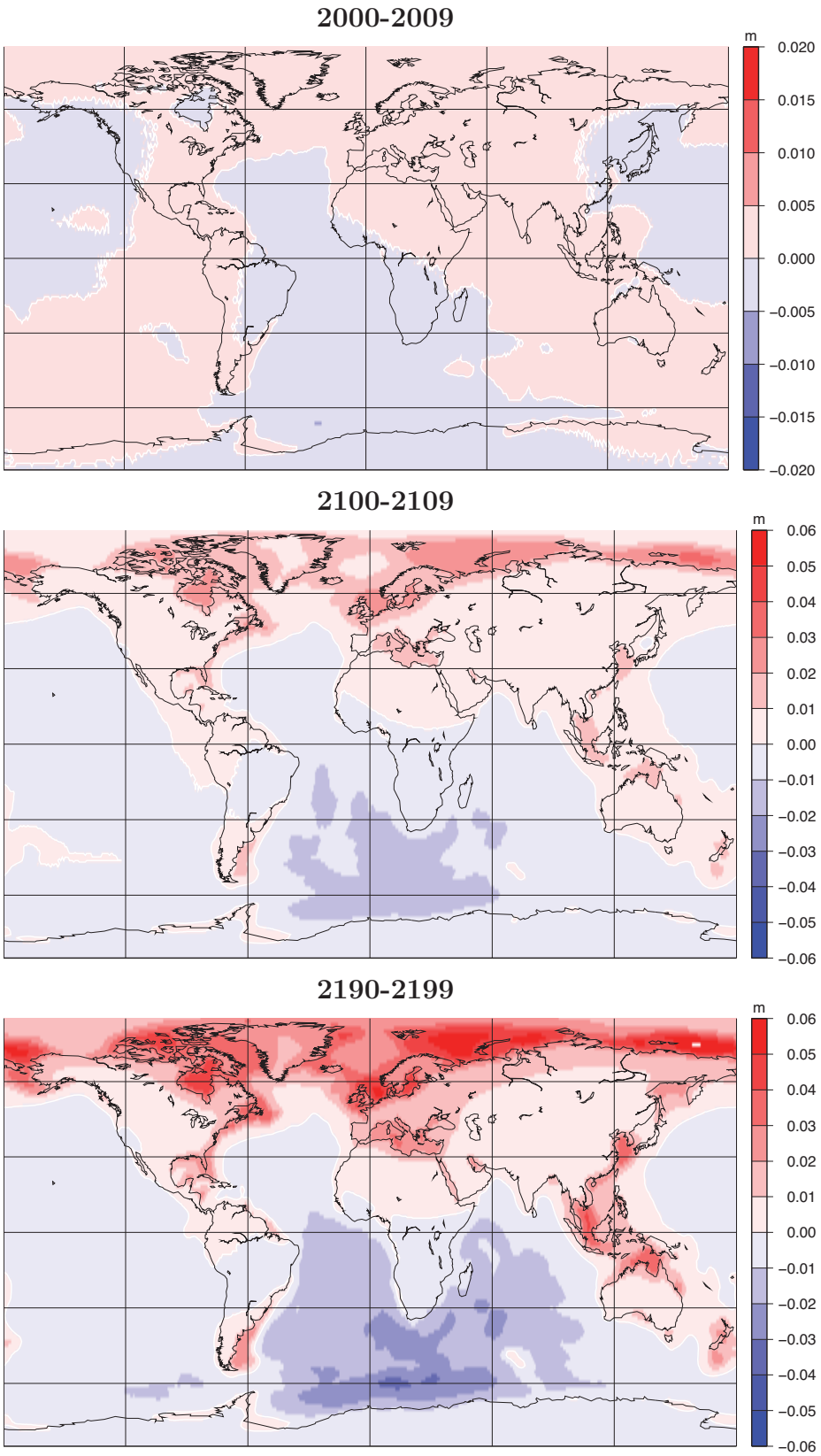

Figure 6.20: Spatial distribution of relative sea-level changes relative to 1860-1869 in meter due to changes in ocean bottom pressure caused by thermal expansion of the A1B IPCC (2001) climate scenario (see Figure E.2 on pages 339-340 for plots over other time periods).

6.6 Summary and conclusions

This chapter addressed some of the possible contributions to eustatic and isostatic sea-level changes. Geodetic signals such as relative sea-level changes and vertical surface deformation are affected by various processes. Apart from tectonics, all other processes discussed here can be described as a redistribution of mass from land to the ocean (or only within the ocean). Hence, the sea-level program *calsea* used previously can also be applied to calculate relative sea-level changes for these processes, provided that relevant input data is available. Overall, the predictions of geodetic signals for all processes show great spatial variability which increases the difficulty of separating the various factors.

Where geodetic signals are calculated in this chapter, estimates showed that, dependent on the location, the geodetic signals at sites caused by the processes described here can be larger than the signal predicted from recent mountain deglaciation. However, in some cases the opposite is determined. Provided that all other contributions to the geodetic observation are known (or negligible), this then allows for a separation of the signal that results from recent mountain deglaciation. The success in constraining the latter process more accurately is strongly dependent on the location of the observing site.